Mohamed Khider University of Biskra
Faculty of exact sciences and natural and life sciences
Material sciences department

MASTER MEMORY

Material sciences
Physic
Condensed material physics
Ref.:

Presented by:
Chenni Chaima
12/06/2024

Preparation and characterization of ZnO-based Schottky diode prepared with sol-gel

---

Jury:

Mis.	Laiadi Widad	MCA	Biskra university	Chairmen
Mis.	Lehraki Nadia	MCB	Biskra university	Examiner
Miss.	Louiza Arab	MCA.	Biskra university	Supervisor

Academic Year: 2024


يا الله
وفقني

Dedication

With pride, I dedicate my work:

And to the one whose brow was covered with sweat and taught me that success does not come to me with patience and persistence, to my beloved father ***"ELHADJ ".***

The joy of your graduation to that great person with the kindest soul and the most beautiful heart, who always wished to see me on a day like this, to my heaven, my mother" ***Mabroka".***

My sister is like the spring of my tenderness, my sister is my heart and its beats. You are the blessing that increased my life.

To my brothers, my lofty mountains are the light of love.

To Mohamed Naufal, my Fiancé, you're my study buddy and soul mate. Thanks for all your hard work with me and pieces of advice.

To the wives of my brothers and lovers of my heart, Juri and Istabrak, Maryam, Adam Esaid.

I do not forget the soul mates who shared the steps of this path with me, to those who encouraged me to persevere and complete the journey, to the companions of the years. I am grateful to all of you.

To my colleagues in Condensed material physics.

Chenni Chaima

Acknowledgements

Inspiration and motivation have always a key role in the success of any venture. First and foremost, praises and thanks to God, the Almighty, for his showers of blessings throughout our research work to complete it successfully.

Above all, I extend special thanks and appreciation to my supervisor in this work, my virtuous professor Louiza Arab, namely professor at the University of Biskra, for his tremendous efforts that she made with me to make this thesis a success, and for her moral support and moral encouragement throughout the completion of this work, so many thanks to her.

I sincerely thank Mrs. Laiadi Widad, a teacher at the University of Biskra who did me the honor of chairing the jury.

My most laudatory thanks to Mrs. Lehraki Nadia, professor at the University of Biskra, who kindly accepted to be part of the jury.

Special thanks to my Ph. D Aya Latif student, who has been supportive in the journey of this work.

Our thanks and appreciation go to Pr. TIBERMACINE Toufik and Dr. SENGOUGA the head chef of laboratory of Metallic and Semiconducting Materials (LMSM) in Mohamed Khider university, and all the members and staff who have willingly helped us out with their abilities in this laboratory.

Table of Content

List of Tables

List of Figures

General Introduction

Transparent conductive films as the name suggests are mainly made from optically transparent and electrically conductive materials called transparent conductive oxide (TCO). TCO films are a class of materials of interest due to their applications in optoelectronics and electronics [1]. A film is a layered material deposit whose thickness is of the order of the wavelength of electromagnetic radiation.

ZnO has been widely studied for its application in the development of transparent electronics. Because of their wide bandgap, zinc oxide-based transparent and conductive films have potential application in multiple areas, including solar cells, photonic crystals, light-emitting diodes, photodetectors, modulator waveguides, varistors, gas sensors, and thin film transistors [2].

The use of TCO materials such as ITO and doped ZnO improves valve transparency and conductivity [3]. Schottky valves are a type of valve based on a metal half-carrier junction and are known for their unique characteristics such as fast switching and high efficiency. The study and development of transparent Schottky diodes using ITO/ZnO configurations prepared by Sol-Gel techniques is a promising field that aims to improve the electrical and optical performance of these devices [4]. By optimizing material properties and preparation techniques, significant improvements in the efficiency and performance of Schottky diodes can be achieved, contributing to the development of the next generation of advanced electronic and optoelectronic devices [5].

This work is divided into three main chapters:

- The first chapter includes general definitions and concepts about transparent oxides, their electrical and optical properties, thermal and chemical stability, and the causes of electrical conductivity in transparent oxides. It also includes a study on zinc oxide, the subject of our research, where its structural, electrical and optical properties are defined, its electronic distribution is mentioned, and finally some possible applications of zinc oxide.
- The second chapter discusses the different techniques used for precipitation, factors affecting the selection of the appropriate precipitation technique, focusing on the Sol-Gel technique (spin coating) as well as thin-film growth mechanisms and characterization techniques.
- Chapter 3: This chapter relates to the experimental work carried out in Laboratory of Metallic and Semiconducting Materials (LMSM) at University of Biskra in

Algeria, and includes the characteristics of the device used in the deposition, how to choose the support and its cleaning method, in addition to the experimental conditions adopted, the preparation of the deposition solutions and the choice of the zinc source, which is zinc acetate. Finally, the chapter reviews the different results obtained, comparing them with previous works and trying to find explanations for these results.

- A general conclusion: This work concludes with a review of the main findings and some future perspectives that can be worked on.

Chapter I: Overview of Transparent Conductive Oxides (TCO): Zinc Oxide (ZnO).

I.1.1. Introduction

In this chapter, we delve into a bibliographic exploration of transparent conductive oxides (TCOs), followed by an examination of zinc oxide (ZnO), including its key properties and applications. Finally, we provide an overview of thin films.

I.2. Transparent conductive Oxides (TCO)

Transparent Conductive Oxides (TCOs) are highly valuable materials for transparent optoelectronics due to their distinctive optical properties in the visible light spectrum. These properties include transparency levels exceedingly approximately 85%, an optical band gap exceeding 3 eV, and adjustable electrical conductivity characterized by carrier concentrations of at least 10^{20} cm^{-3} and a resistivity of around 10^{-4} Ω·cm.

I.3. Definition of TCO

Transparent conducting oxides (TCOs) are electrically conductive materials with comparably low absorption of electromagnetic waves within the visible region of the spectrum [6].

I.4. Properties of TCO

I.4.1. Optical Properties

The optical properties depend on the interaction of the electromagnetic wave with the electrons of the material [7]. Optical transmission is characterized by the relationship between the intensity of the incoming light and that transmitted through the material concerned [8], The optical properties of materials are governed by three essential phenomena which are transmission, reflection and absorption, these phenomena being characterized by parameters T (transmittance or transmission factor), R (reflectance or reflection factor), A (absorbance or absorption factor) and α (absorption coefficient) [9].

I.4.1.1. Reflectance

Reflectivity R is the ratio between the intensity of the reflected optical beam and the intensity of the incoming optical beam expressed in the following relationship:

$$R = I_r / I_0 \qquad \text{(I-1)}$$

I.4.1.2. Absorbance

The ratio between the intensity of the absorbed optical package and the intensity of the incoming optical package is expressed for:

$$A = I_A/I_0 \quad \text{(I-2)}$$

I.4.1.3. Transmittance

Ratio between the intensity of the optical beam window through the material on the intensity of the visual beam received is expressed in the following relationship:

$$T = I_T/I_0 \quad \text{(I-3)}$$

Thus, the total of three phenomena is equal to 1.

$$T + A + R = 1 \quad \text{(I-4)}$$

I.4.1.4. Absorption coefficient

The Beer-Lambert law makes it possible to relate these phenomena by the equation [10]:

$$T = (1 - R)e^{-i\alpha d} \quad \text{(I-5)}$$

T: the transmission coefficient.

R: the reflection coefficient.

d: the thickness of the film considered.

α: the absorption coefficient depending on the wavelength λ.

I.4.1.5. Extinction coefficient

The extinction coefficient represents the amount of energy absorbed by the substance, i.e. the extinction of the wave Electromagnetic, meaning energy loss due to the interaction between wave and material and other factors that cause loss of wave energy; we can calculate the extinction coefficient with the following relationship [10]:

$$K = \alpha\lambda/4\pi \qquad \textbf{(I-6)}$$

I.4.1.6. Merit coefficient

This coefficient that connects optical and electrical properties and this coefficient is defined as the ratio between medium permeability in the visual field (800nm-400nm), on surface resistance [10]:

$$I_{TC} = T_m/Rs \qquad \text{(I-7)}$$

T_m: Optical Transmittance.

R_s: Surface Resistance.

The transmission properties of TCO are defined by depending on the wavelength λ, as illustrated in figure (I-1).

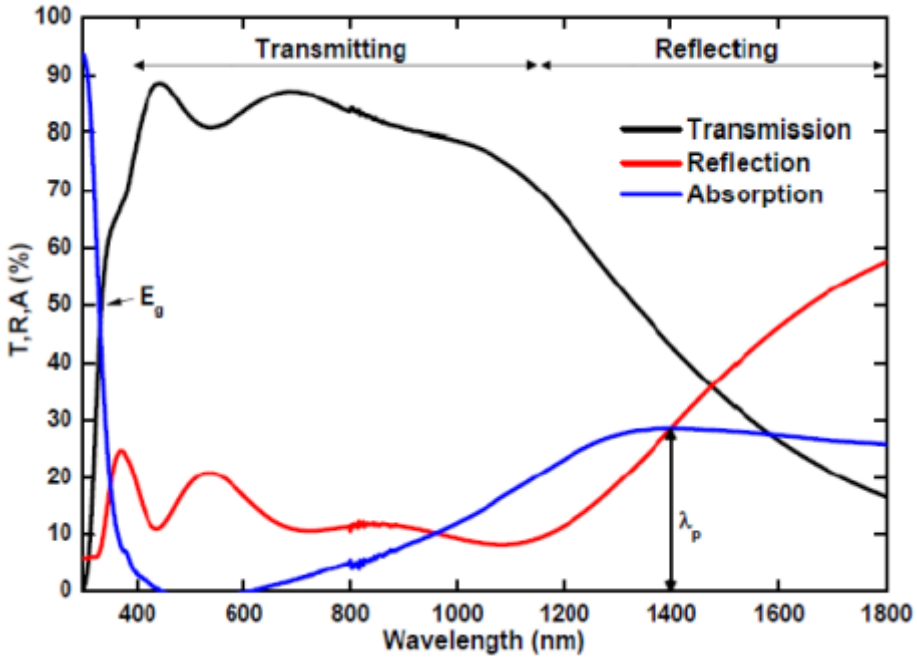

Figure I-1: Transmission, Reflection and absorption spectra of a typical TCO [11].

The transmission characteristics of TCOs are highly specific and generally remain consistent across different TCO materials, with minor variations based on their unique properties. This can be broken down into three main components [11]:

- A strongly absorbing region in the short wavelength spectrum, attributed to band-gap excitation of the oxide.
- A transparent region within the visible spectrum.
- A reactive region beyond a certain wavelength in the infrared (IR) range, due to the presence of free carriers.

These characteristics are illustrated in Figure (1). While the transmission within the visible spectrum may experience slight attenuation due to the absorption of unreacted species within the oxide or scattering at rough surfaces, it typically remains above 80%. Smooth film surfaces exhibit a distinctive periodic fluctuation in transmission [11].

I.4.2. Electrical Properties

Transparent conductive oxides have undergone a study on their electrical properties since the 1970s [12]. The electrical properties of these semiconductors are comparable to those of large gap semiconductors. Semiconductor materials known as TCOs exhibit a wide gap (Eg) and electrical conductivity that ranges between 10^{-4}-10^{5} ($\Omega.cm^{-1}$) [13]. It's important to note that electrical conductivity $\boldsymbol{\sigma}$ in TCOs comes from intrinsic defects like oxygen vacancies and interstitial atoms of the metal or extrinsic dopants [14]. It is conveyed by :

$$\boldsymbol{\sigma = \frac{1}{\rho} = q.n.\mu} \qquad \textbf{(I-8)}$$

σ: Electrical Conductivity.

n : Charge carrier Density.

μ: Mobility of load carriers.

q: Elementary electric charge of the electron.

I.5. Criteria for Choosing TCO

The ideal over-the-counter (TCO) material for optoelectronic purposes, like photovoltaic cells, should possess excellent optical transparency within the visible spectrum and exhibit high electrical conductivity. Other factors such as thickness, deposition temperature, toxicity, and manufacturing cost can also play a significant role in determining the appropriate choice of conductive transparent material for specific applications. For

instance, the limited applicability of ITO in flexible electronics stems from the susceptibility of its thin films to fragility. In comparing different Transparent Conductive Oxides (TCOs), Haacke introduced a metric known as the merit factor (F_{TC}), which is a ratio between transmittance (T) and square resistance (Rs). This merit factor (F_{TC}), expressed in units of Ω^{-1}, it is calculated using the relationship [15]:

$$F_{TC} = \frac{T^{10}}{R_S} \quad \textbf{(I-9)}$$

$$R_s = \frac{\rho}{d} \quad \textbf{(I-10)}$$

Where:

ρ: resistivity.

d: thickness.

R_s=sheet resistance.

I.6. Applications of TCOs materials

Transparent conducting oxide (TCO) films have found extensive application due to their luminescent characteristics. They are utilized in a variety of fields including solar cells, flat panel displays, smart windows, touch screens, optoelectronic devices, heat mirrors, liquid crystal displays (LCDs), organic light emitting diodes (OLEDs), gas sensors [16], …. etc. as shown in figure I-2.

Figure I-2: Some applications of TCOs [16].

I.7. Nanomaterials

Nanomaterials are defined as a group of substances with at least one dimension less than about 100 nanometers. The nanometer is equivalent to 0.000001 millimeter. - about 100,000 times smaller than the diameter of a human hair. Nanomaterials are interesting because on this scale, unique optical, magnetic, electrical and other properties appear. These emerging properties have the potential to have significant effects in electronics, medicine and other fields [17].

Figure I-3: Nanomaterial (For example: Carbon nanotube) [17].

I.8. Classification of nanomaterials

Nanomaterials have an extremely small size that has at least 100 nanometers or less away. Nanomaterials can be nanoscale in one dimension (e.g. surface membranes), two dimensions (e.g. threads or fibers), or three dimensions (e.g. particles). They can be found in simple, fused, assembled or grouped forms in spherical, tubular and irregular forms. Common types of nanomaterials include nanotubes, dendrites, quantum dots and folerins. Nanomaterials applications in nanotechnology show different physical chemical properties from ordinary chemicals (i.e. nanoscale silver, carbon nanotubes, folerin, photostimulator, nanocarbon, silica) [17].

According to Siegel, Nanostructured materials are classified as Zero dimensional, one-dimensional, two-dimensional, three-dimensional nanostructures (Figure I-4) [18].

- Nanomaterials (0D): none of the three dimensions of which is greater than 100 nm, these are nanomaterials having a dispersed, random or organized form, for example: clusters, nanoparticles, fine powder whose grains are almost spherical.

- Nanomaterials (1D): one of the dimensions is greater than 100 nm, as nano-wires, nano-tubes and nanorods.

- Nanomaterials of dimension (2D): two of the dimensions are greater than 100 nm, such as thin film materials or nanosheets.

- Nanomaterials (3D): the three dimensions are greater than 100 nm.

The nanoparticles or nano-objects are incorporated together to form a new well organized and frequent or random matrix; this allows to modify their properties, mechanical, optical, magnetic, etc., and therefore this matrix can bring a new feature. They are called nanocomposites.

NB: Nanomaterials (1D) and (2D) are called nanostructures or nanometers [19].

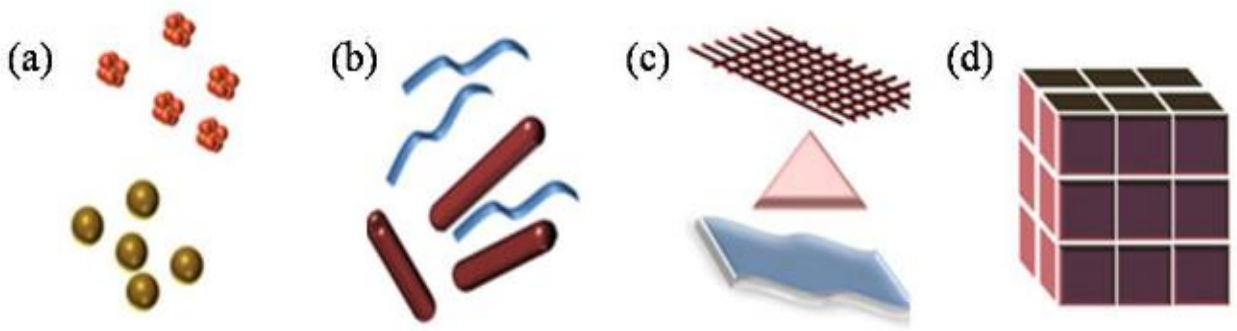

Figure I-4: Classification of Nanomaterials (a) 0D spheres and clusters; (b) 1D nanofibers, nanowires, and nanorods; (c) 2D nanofilms, nanoplates, and networks; (d) 3D nanomaterials [17].

I.9. Thin films

In principle, a thin layer of a given material is an element of this material in which one of its dimensions, the so-called thickness, has been greatly reduced, so that the small distance between the two boundary surfaces remains of the order of μm, giving the layer quasi-bidimensionality, which leads to a disruption of the majority of physical properties. The essential difference between bulk and thin-film materials is that, in the bulk state, the role of the boundary surfaces in the properties is generally rightly neglected, whereas in the thin film state, the effects of the boundary surfaces are predominant. It's quite obvious that the thinner the layer, the greater the two-dimensional effect. However, once the thickness exceeds a

certain threshold, its effect will become minimal and the material will regain the well-known properties of solid material [20]

I.10. Thin films growth process

Understanding the growth mechanism of thin films at the atomic level is fundamental to both the science and technology of thin films especially with our increasing desire to obtain thin films with excellent properties; It is well known that the factors controlling: nucleation, growth, structural development, crystallization, as well as the physical properties of the slides are: thin film material, flow, kinetic energy of atoms and molecules on the surface of the support, growth temperature, contaminant flux and datum-related factors such as: constituent materials, surface cleanliness, crystallization, direction of crystallization [21].

Regardless of the material or deposition method, the thin film growth mechanism proceeds through the following main stages:

- Condensation and nucleation of atoms on the surface.
- Docking (nuclear growth).

I.10.1. Growth modes

Three basic patterns have been identified for the growth of a thin film on a support [22]:

- Island pattern (three-dimensional or multi-layered) called the Weber-Volmer pattern.

- Layer-by-layer (two-dimensional) pattern called the Frank Frank-van der Merwe pattern.

- Mixed mode is called the Krastanov-Stranski mode.

Three modes of growth are schematically illustrated in the figure (I-5):

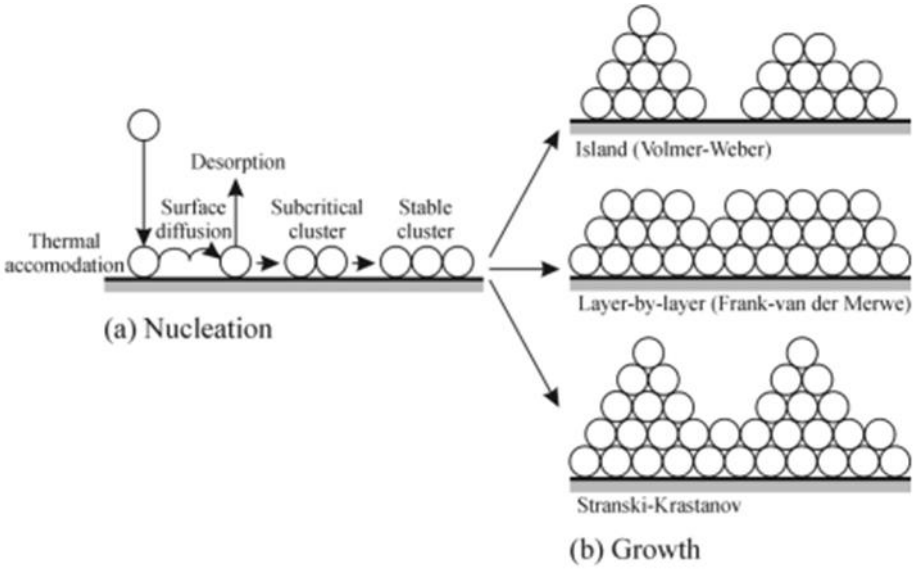

Figure I-5: Schematic representation of (a) the steps leading to nucleation and (b) the three film growth modes [21].

I.11. Zinc oxide (ZnO)

ZnO is not a recent addition to the semiconductor field. Research on its growth techniques and material properties dates back to 1912. Following the transistor's invention and the onset of the semiconductor era, the lattice parameters of ZnO were established by 1935, with detailed optical parameter values becoming available in the mid-1950s. Systematic studies on ZnO as a compound semiconductor were conducted in 1960 (Fig. (I-6) [14].

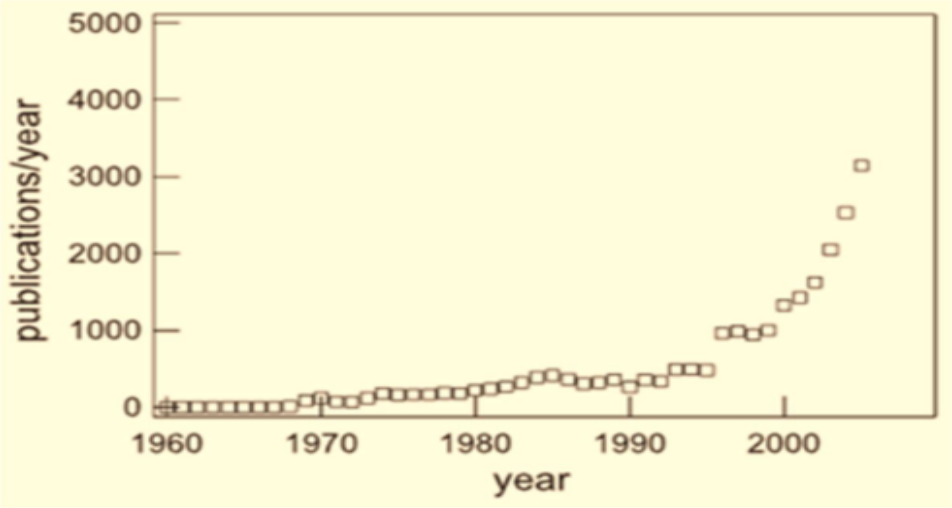

Figure I-6: Increase of the number of publications about zinc oxide according to the literature data base SCOPUS [14].

Zinc oxide is a member of the Transparent Conductive Oxides (TCO) family. The non-toxicity and abundance on earth of this compound make it an ideal candidate in several areas. It has very diverse properties used for centuries in many fields, from paint to roofs, piezoelectric sensors to cosmetics. Below, we briefly show the various well-known properties of zinc oxide, whether from a crystallographic, electrical and optical point of view. Zinc oxide can exist in nature in the form of powder or solid crystal. It comes in the form of mineral. It is a direct wide band gap semiconductor whose color varies according to the impurities it contains (its red color for example, is due to the presence of manganese within the material; pure, it is transparent) and according to its deviation from the stoichiometry[23].

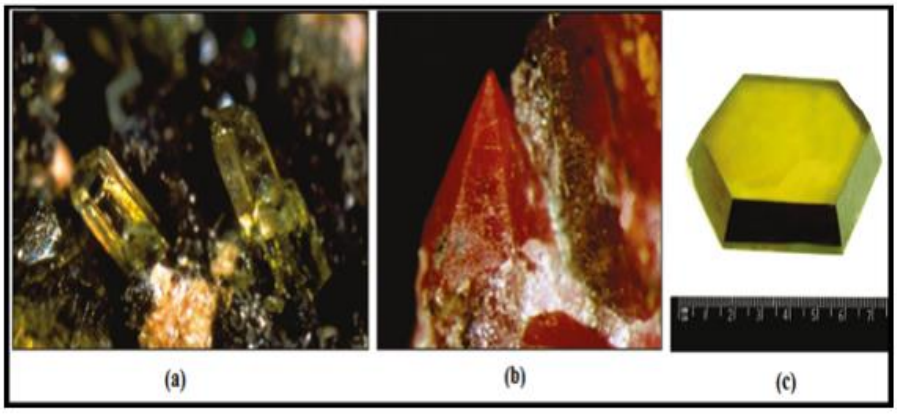

Figure I-7: Massive ZnO in its natural form (a) and (b), coming from hydrothermal synthesis (c) [24].

I.12. Why chose ZnO specifically?

ZnO is a wide bandgap semiconductor (3.37 eV at 300K), it is transparent in the visible and near infrared (IR). The main advantages of ZnO are [25]:

- ✓ High luminescent efficiency, non-ohmic, and non-toxic.
- ✓ High exciton energy (60 meV).
- ✓ ZnO can be prepared at a lower temperature.
- ✓ High piezoelectric effect (e_{33} = 1.2 C/m^2).
- ✓ High thermal conductivity (K = 0.54W. cm^{-1}. K^{-1}).
- ✓ Drift mobility that saturates at higher fields than GaN (attractive for devices with high frequency).

- ✓ A very high shear module (45.5 GPa) which indicates crystal stability (for example: 18.35 GPa for ZnSe, 32.6 GPa for GaAs, 51.37 GPa for Si).
- ✓ Very abundant on Earth.
- ✓ Enthalpy training is $6.5x10^5$ $J.mol^{-1}$.
- ✓ Melting temperature is greater than 2250 K.
- ✓ Its density is 5675 $Kg.m^{-3}$.

I.13. Properties of zinc oxide

Zinc oxide is a partially soft material with a density of about 5.6 $g.cm^{-3}$ and a melting temperature greater than 1800°C. This material, which consists of 80.34% zinc (Zn) and 19.66% oxygen (O), can be plastically deformed at low loads [26]. Its main mechanism of deformation is the sliding according to the basic planes (perpendicular to the axis c) and the pyramidal planes. ZnO in thin films can be considered hard compared to solid ZnO, with a hardness of 5.75 GPa and a Young module of 310 GPa [27]. The main mechanical properties of ZnO wurtzite oriented along axis c [28] are presented in Table 1.1.

Table I-1 : Some mechanical properties of ZnO [23].

Parameter	Value
Young's module (GPa)	111.2
Hardness: H (GPa)	5.0
Mass coefficient: B (GPa)	[142 – 183]
$\boldsymbol{e_{33}(C, m^{-2})}$	1.32
$\boldsymbol{e_{31}(C, m^{-2})}$	[–0.51, –0.66]
$\boldsymbol{e_{15}(C, m^{-2})}$	–0
$\boldsymbol{d_{33}(C, m^{-2})}$	11.7
$\boldsymbol{d_{31}(C, m^{-2})}$	- 5.43
$\boldsymbol{d_{15}(C, m^{-2})}$	–11.3
$\boldsymbol{\alpha(10^{-6}/K)}$	2.92

Spontaneous polarization (cm^{-2})	−0.047

I.13.1. Structural properties of ZnO

Zinc oxide (ZnO), also called zincite when found naturally, can be present either as a powder or as a solid crystal. Table I.2 lists some general properties of ZnO [29].

Table I-2 : Some properties of ZnO.

General description	Density (g/cm3)	Molecular density (molecules/cm3)	Melting point (C°)	Enthalpy of formation (kcal/mole)	Solubility in H2O at 29 C° (g/l)
Colorless crystals, white powder [26]	**5.60 [26]**	**4.21x1022 [26]**	**1975**	**83.17**	**0.0016**

Three different crystallographic phases are currently known for zinc oxide: phase (Wurtzite), phase (Blende) and phase (Rocksalt).

The hexagonal “Wurtzite” structure: thermodynamically stable at room temperature.

The Cubic “Zinc Blende” structure: is observed when ZnO is deposited on certain cubically symmetrical substrates.

The Cubic “Rocksalt” structure: obtained when hydrostatic pressure is applied to the Wurtzite structure. These different structures are shown in Figure (I-8)

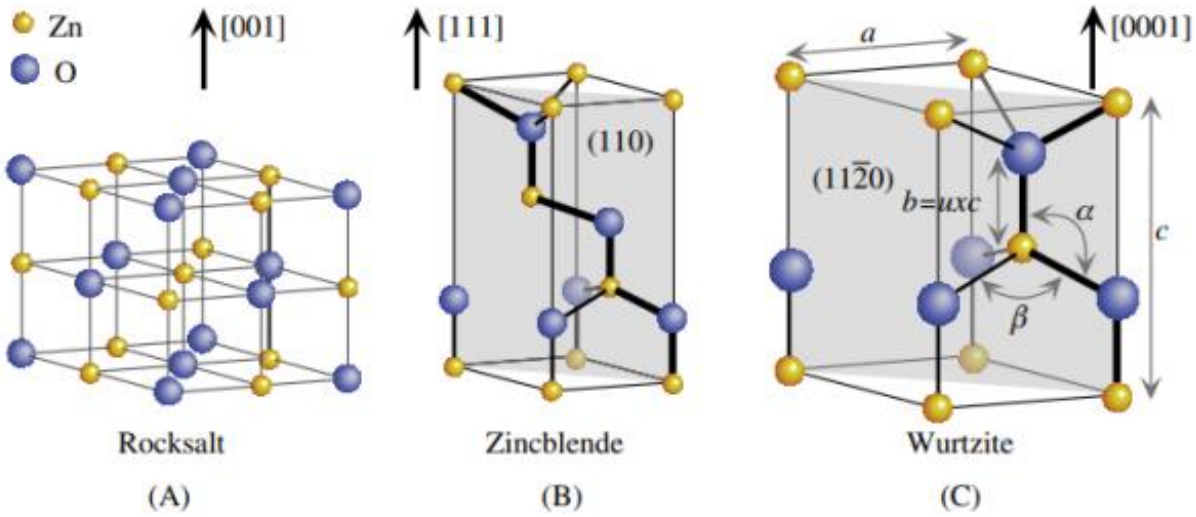

Figure I-8: ZnO crystal structures: (a) Cubic rock salt, (b) Cubic zinc blend, (c)Hexagonal wurtzite (Zinc atoms in gray and oxygen in black).

Each Zn atom is surrounded by four oxygen atoms, with the yellow spheres representing the Zn atoms and the ones Violet the oxygen atoms.

Under standard conditions, the "Wurtzite" structure is the most thermodynamically stable. Whereas "Zinc Blende" is only obtained in the case of growth on cubic substrates and the "Rocksalt" structure is only obtained under relatively high pressure [30].

The figure (I-10) shows the distribution of Zn and O atoms to form the crystallographic Wurtzite crystallographic structure of ZnO.

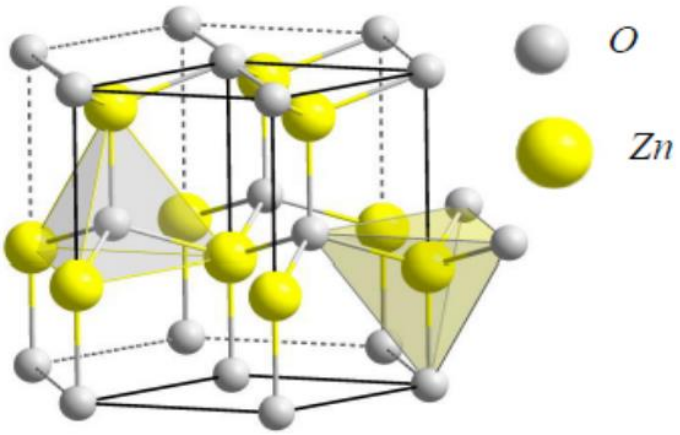

Figure I-9 : Primitive cell of the Wurtzite phase of ZnO [30].

The Wurtzite structure contains two zinc atoms per cell. Each zinc atom is surrounded by four oxygen atoms and vice versa, giving a coordination of 4.

The table below presents a summary of some structural characteristics of zinc oxide.

Table I-3: Main characteristics of the wurtzite structure of ZnO [25].

Structure		**Hexagonal Wurtzite**
Angle		$\alpha=\beta=90°$ $\gamma= 120°$
Lattice parameters(T=300K)		a_0=0.32495(nm) c_0=0.52069(nm) a_0/c_0=1.602 (1.633 in an ideal wurtzite structure)
Atomic position		Zn: 2/3, 1/3, 0 ;1/3, 2/3, 1/2 O: 2/3, 1/3, µ; 1/3,2/3, 1/3^{+}µ and µ=3/8
Ionic ray for a coordination tetrahedral	Covalent bond	Zn neutral = 1.31 Å O neutral = 0.66 Å
	ionic bond	Zn^{+2}=0,06 O^{-2} =1,38 Å
Distance between$O^{-2}$and Zn^{+2} (nearest neighbors)		According to axis c d=1.96Å, For the other three of 1.98Å
Crystalline ray for coordination Tetrahedral		Zn^{+2}=0,74Å O^{-2}=1,24 Å

When a material is reduced to nanometric dimensions, the quantum confinement effect caused by the size reduction results in significant changes in the physical characteristics of the substance.

Of all the materials, ZnO probably has the most diverse family of nanostructures. The

different forms of nanoparticles that have been produced from ZnO powder are noncoms, nanoring's, nano springs, nano bows, nanobelts and nanowires. These nanostructures are illustrated in Figure I-11.

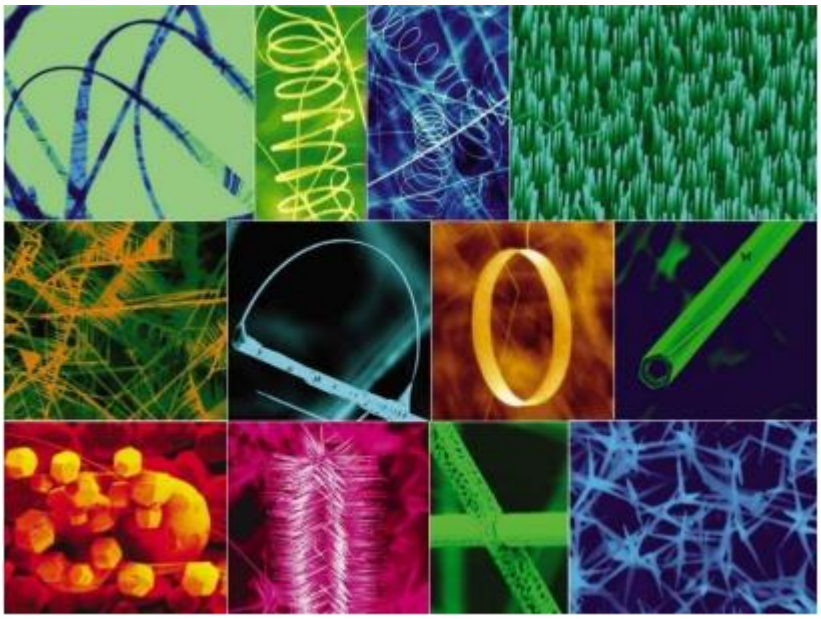

Figure I-10: Different forms of ZnO nanostructures [31].

I.13.2. Electrical and electronic properties

The electronic structure of the zinc and oxygen is:

$$O : 1s^2 2s^2 2p^4$$

$$Zn : 1s^2 2s^2 2p^6 3s^2 3p^6 3d^{10} 4s^2$$

The fabrication of high-quality p-type ZnO films has posed challenges, primarily attributed to defects resulting from stresses induced by dopants in the crystal. Calculations have shown remarkably low formation energies for oxygen vacancies and zinc interstitials in ZnO, which are likely responsible for the inherent n-type conductivity observed in freshly grown films [32]

Theoretical calculations and experimental results concerning the band structure of zinc

oxide (ZnO) are presented in figure (I-11). It shows the calculated band structure of Wurtzite crystal of ZnO. Different theoretical approaches have been used to determine the band structure, revealing that ZnO is a direct bandgap semiconductor. The Zn 3d levels were localized using local density approximation (LDA) and self-interaction-corrected pseudopotential integration (SIC-PP). The band structure indicates the energy states of the zinc and oxygen atoms, with the band gap calculated at 3.77 eV. Experimental studies using electron energy loss spectroscopy (EELS) and UV photoelectron spectroscopy confirm the theoretical results and indicate differences in electronic properties between the Zn and O faces in ZnO wurtzite [33].

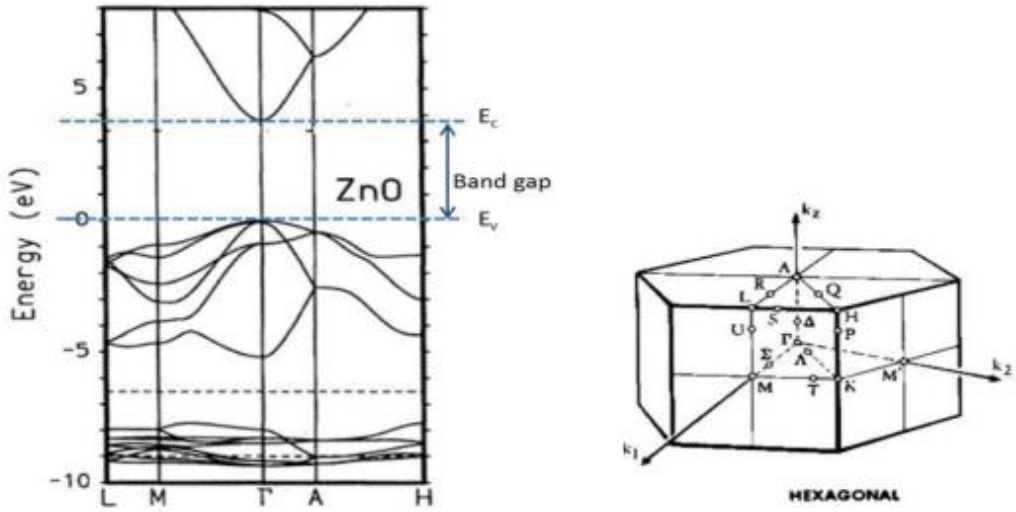

Figure I-11: Local density approximation of the band structure of bulk ZnO [33].

The Hall Effect measurements determine the electrical characteristics of ZnO thin films, including electrical resistivity, charge carrier concentration, and mobility. The resistivity (ρ) of an n-type thin film is contingent upon both the electron density (n) within the conduction band

and their mobility (μ), with e representing the electron charge, a constant value:

$$\sigma = \frac{1}{\rho} = en\mu_n \qquad \textbf{(I-11)}$$

ZnO has a relatively large direct band gap of ~3.3 eV at room temperature; therefore, pure ZnO is colorless and transparent. Advantages associated with a large band gap include higher breakdown voltages, ability to sustain large electric fields, lower electronic noise and high temperature and high-power operation. The bandgap of ZnO can further be tuned from 3~ 4 eV by its alloying with magnesium oxide or cadmium oxide [34].

The n-type character of most zinc oxide (ZnO) without intentional doping, attributing it to native defects like oxygen vacancies or zinc interstitials, or possibly unintentional substitution by hydrogen impurities. It mentions the ease of achieving controllable n-type doping by substituting Zn with group-III elements. Reports suggest that resistivity and mobility in ZnO films are largely independent of the deposition method, with values around 2×10^{-4} Ω.cm and 50 $cm^2/V.s$ respectively. However, achieving p-type ZnO is challenging due to limited solubility of p-type dopants and compensation by n-type impurities. Measurement of p-type conductivity in n-type material is also difficult due to inhomogeneity. High levels of p-conductivity in ZnO have yet to be experimentally confirmed [34]

Table I-4: Physical properties of the zinc oxide in the wurtzite form [35].

Property	Values
Nature of the band gap	Direct
The band gap at **300 °K** (**eV**)	$\mathbf{3.34 \pm 0.02}$
Conductivity type	***n and* (*p*)**
Electrical conductivity ($(\mathbf{\Omega.cm})^{-1}$)	$\mathbf{10^{-6} - 10^{2}}$
Charge carrier density ($\mathbf{cm^{-3}}$)	10^{15} -10^{21}
Density of states in CB ($\mathbf{cm^{-3}}$)	3.71×10^{18}
Density of states in VB ($\mathbf{cm^{-3}}$)	1.16×19^{19}
Electrons mobility ($\mathbf{cm^2/V.s}$)	0.2-200
Holes mobility ($\mathbf{cm^2/V.s}$)	5-50
The effective mass of electrons	0.28 m_0

The effective mass of holes	0.60 m_0
Thermal velocity of electrons (**cm. s^{-1}**)	2.2×10^7
Thermal velocity of holes (**cm. s^{-1}**)	1.5×10^7
Relative dielectric constant $\varepsilon_r = \frac{\varepsilon}{\varepsilon_0}\ t$	$\varepsilon_{\parallel}$=8.7 $\varepsilon_{\perp}$=7.8

I.13.3. Optical properties and luminescence

Zinc oxide is a transparent material with a refractive index as large as 2 in the bulk state, and as a thin film, it has a refractive index between 1.90 and 2.20; there is a relationship between defect density and forbidden bandwidth on the one hand and between defect density and absorption coefficient on the other hand, whereby a decrease in defect concentration leads to an increase in the forbidden bandwidth and decreases the absorption coefficient [20].

Under the influence of a high-energy light beam (3.4 eV < E) or electron beam bombardment, zinc oxide emits photons, where UV emission has been observed and is due to the binding of an electron from the conduction band with a hole from the valence band, and emission in the visible range such as violet, blue and green light. Blue and green light due to intrinsic defects; green light is due to energy level transitions of oxygen vacancies, while blue and violet are due to energy level transitions of zinc vacancies and the interfacial levels of zinc atoms. This allows us to use zinc oxide in the optoelectronic industry: UV light diodes and UV lasers [20, 32].

The luminescence varies with the doping of the material, and this property is exploited in various optoelectronic devices such as cathode ray tube displays and light-emitting diodes used in color display, signaling, and lighting. Recently, special attention has been paid to the emission of ZnO films due to their high luminescence efficiency, non-ohmic property, and high excitation energy (60 meV). The latter energy is higher than that of materials such as ZnS (20 MeV) and GaN (21 MeV). In addition, ZnO can be prepared at lower temperatures than these other two materials [7].

I.13.4. Review of doped zinc oxide thin films

Dopers such as Al, In, As, S, Sn, Mn, and others are used in ZnO thin films for a range of applications. These dopants allow control of electrical, optical, and magnetic properties, making doped ZnO films attractive for use as transparent conductors with high visibility and conductivity. Despite industry standards such as ITO and FTO, there is considerable interest in discovering more economical and stable alternatives [36].

Table summarizes doped films, including their transmittance in the visible range and lowest resistivity values. Typical dopants used to enhance ZnO conductivity include group III (B, Al, In, Ga) and group IV (Pb, Sn) elements from the periodic table.

Table I-5: Summary of different doped ZnO thin films as transparent conductors [36].

Dopant	Methods	Transmittance in visible range	Lowest resistivity
Al	Pulsed laser deposition (PLD)	~90%	$\sim 10^{-4}$ Ωcm
	Radio-frequency (RF) magnetron sputtering		
	Solution processed		
Ga	PLD	~85%	$\sim 10^{-3}$ Ωcm
	Solution processed		
In	Solution processed	~80%	~20 Ωcm
N	Plasma-assisted molecular beam epitaxy	~80%	$\sim 10^{-2}$ Ωcm
	RF magnetron sputtering		
	Solution processed		

I.14. Zinc oxide applications

Zinc oxide has many scientific, industrial and high-tech applications, so zinc thin films are widely used in various applications.

I.14.1. Transparent conductive oxides

Transparent conductive oxides (TCO) are commonly used as electrodes in various optical and electronic devices such as displays, solar cells, LEDs, and OLEDs. Indium tin oxide (ITO) is favored for its transparency and exceptional conductivity, but its limited availability makes it expensive. Zinc oxide (ZnO) is a promising alternative due to its widespread availability, ease of obtaining, and good transparency and conductivity in the visible spectrum. Although the conductivity of ZnO is not on par with ITO, it can be enhanced by doping with elements such as Al, In, and Ga. Research by Agura et al. and John et al. has shown that Al-doped and Ga-doped ZnO thin films exhibit low resistivity, with reported values similar to ITO transparency [30,37].

I.14.2. Gas Sensors

The importance of gas sensors in various applications such as environmental monitoring, fire detection, and industrial safety. It emphasizes the advantages of semiconductor oxide-based gas sensors, especially ZnO thin film sensors, due to their ease of fabrication, low cost, and high sensitivity to adsorbed gases. Doping ZnO with suitable elements enhances surface density and porosity, which improves sensing selectivity and response time, especially at high temperatures. Several reports detail ZnO gas sensors, such as ammonia, nitrogen dioxide, carbon monoxide, and ethanol, with examples including ZnO-doped aluminum-doped ZnO for ethanol sensing and ZnO-doped Sn-doped ZnO for nitrogen dioxide detection. Other reported work includes diode-doped ZnO sensors for hydrogen detection and thin-film ZnO sensors for the detection of multiple gases such as H2, NO2, and hydrocarbons. In addition, there is mention of p-type ZnO thin-film sensors for NH3 detection achieved by co-doping with aluminum nitride and aluminum arsenide [30, 37].

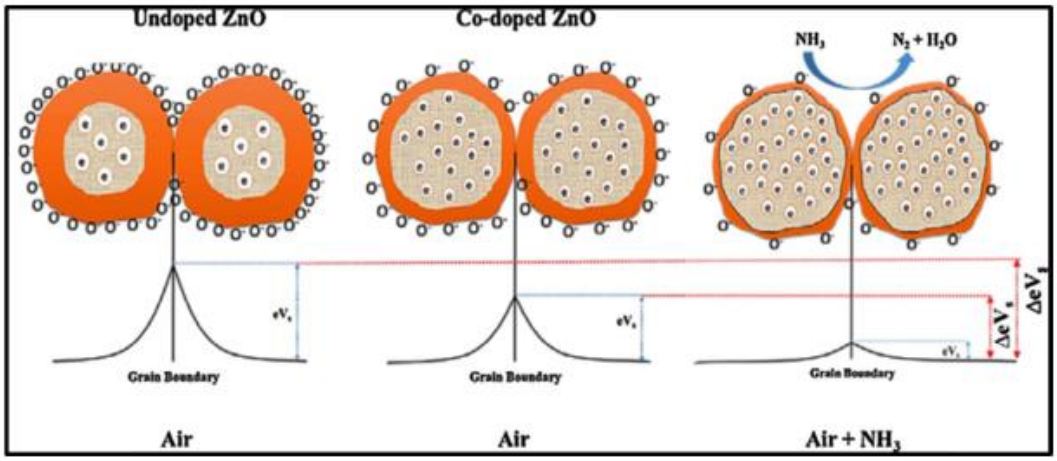

Figure I-12: Schematic diagram of undoped ZnO and Co-doped ZnO thin films for Ammonia gas sensing [38].

I.14.3. Light-Emitting Diodes

The potential of ZnO for blue and UV LEDs is due to its favorable properties such as large band gap and high exciton energy. Its cost-effectiveness compared to GaN is also advantageous. However, the main obstacle in the development of ZnO LEDs has been the lack of stable p-type ZnO. An alternative involves the use of n-type ZnO on other p-type materials. Several ZnO-based heterojunction LEDs have been created, covering the UV, visible and even infrared bands. Examples include UV LEDs synthesized through PLD and CVD methods, blue LEDs via MOCVD and CVD processes, and red LEDs using diverse structures such as n-ZnO/n-ZnMgo/n-CdZnO/p-ZnMgo. Greenish-white LEDs and infrared LEDs have also been realized using innovative fabrication techniques [39].

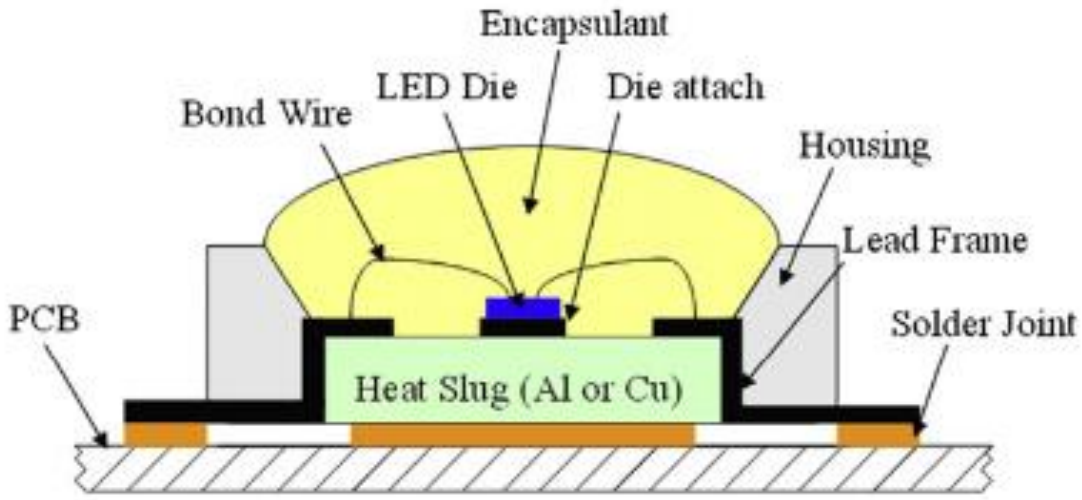

Figure I-13: LED package assembled with printed circuit board (PCB) [39].

I.14.4. Photoconductor

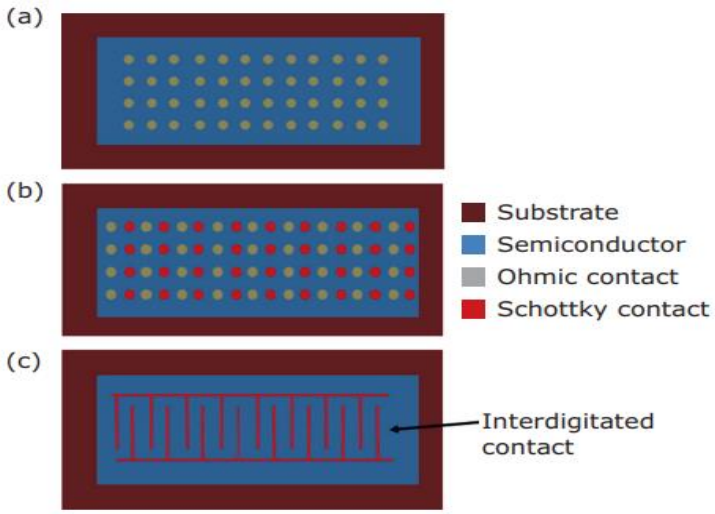

Figure I-14: ZnO based: (a) photoconductor; (b) MSM photodiode; (c) Schottky photodiode.

The figure (I-14) shows the structure of a ZnO photoconductor. It is very simple to fabricate. The ohmic contacts are patterned over a ZnO thin film layer. For ohmic contacts, Al, Ti and ITO can be used. A ZnO based photoconductor exhibits high internal gain. The disadvantage is that it exhibits a very high dark current. The responsivity and linear dynamic range are also low [36].

I.14.5. Schottky Photodiode

The structure and benefits of a ZnO-based Schottky diode, and its advantages over other photodiodes are low dark current, high speed, and high quantum efficiency. Early attempts in 1986 showed limited efficiency, but subsequent efforts have focused on improving it. Commonly used metals for Schottky contacts include Pd, Au, and Pt due to their stability with ZnO films, while aluminum is often used for ohmic contacts.

Recent advances include the work of Tang et al. using a ZnO nanofilm coated on an array of graphene nanodots for UV detection, resulting in enhanced efficiency. In addition, Su et al. developed a high-performance, self-powered beryllium zinc oxide-based dual-color UV photodetector with ultrafast response speed and two response wavelengths corresponding to the UVA and UVB regions [40].

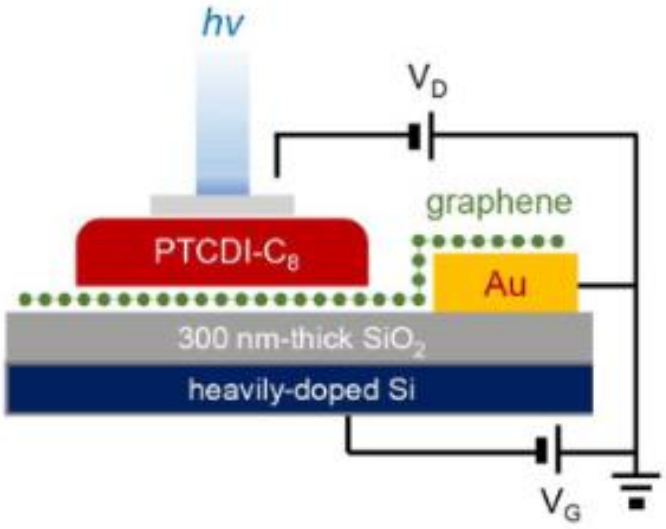

Figure I-15: Schematic device structure of Schottky junction photodiode [40].

They are also used in voltage stabilization applications to prevent the transistor from reaching saturation, and are used in TTL digital elements because these elements require a high switching speed (opening and closing). Schottky diodes are an important component in digital computers, as the performance of the computer depends on the speed at which the diodes are switched.

I.14.6. pn Homojunction Diode

There are very few reports on ZnO-based pn homojunction UV detectors due to difficulty in achieving p-type ZnO thin films as discussed earlier. But a few groups like Liu et al, Moon et al. and Chiu et al. have succeeded in growing stable p-type ZnO thin films and have reported ZnO based pn homojunction UV detectors. ZnO was doped mainly with As, nitrogen or antimony to achieve p-type conductivity (fig. I-16) [41].

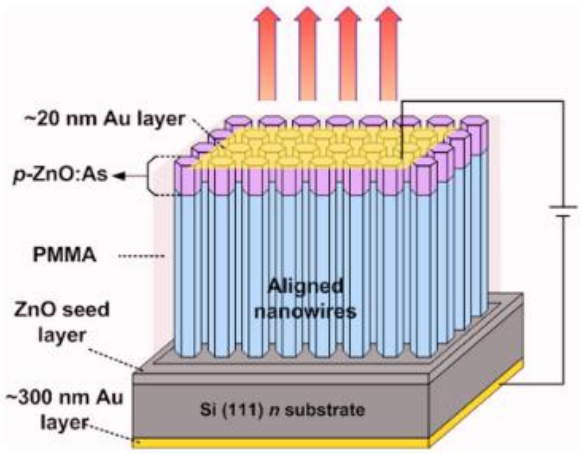

Figure I-16: Schematic illustration of the p-ZnO: As/ n-ZnO NR homojunction device on Si substrate [41].

Chapter II: Thin films deposition methods and characterization techniques

II.1. Introduction

This chapter contains the deposition methods of thin films, whether physical or chemical types, followed by the characterization techniques.

II.2. Deposition methods of thin films

Deposition processes are generally classified into two main families: chemical and physical processes as shown in figure (II-1):

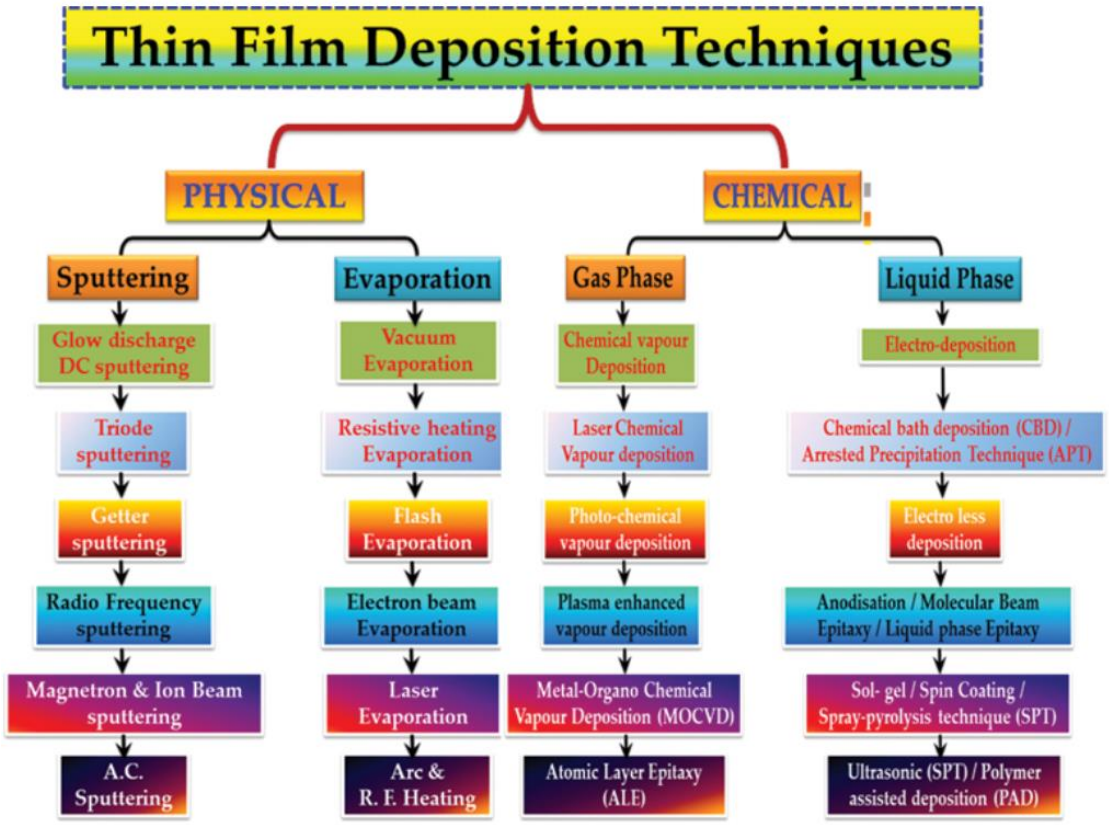

Figure II-1: Classification of thin film techniques [42].

II.3. Choice of a deposition technique

The choice of deposition technology is mainly determined by the quality of the thin films produced and their application. First, it is important which technique will be used to produce the material to be deposited. Factors that influence the choice of technology are [43]:

- ✓ The nature of the material to be deposited.
- ✓ The desired deposition rate and layer thickness.
- ✓ Constraints imposed by the substrate.
- ✓ The desired stoichiometry.

- ✓ The adhesion of the deposit to the substrate.
- ✓ The reproducibility and the cost of realization.

II.4. Physical Processes

II.4.1. Physical Vapor Deposition (PVD)

PVD technology is very versatile, enabling one to remove virtually all types of inorganic materials, such as metals, alloys, compounds, and mixtures, as well as some organic materials. PVD coatings are generally used to demonstrate hardness, corrosion resistance, and oxidation resistance. Therefore, these coatings are used in a wide range of applications such as: aerospace, automotive, surgical/medical, dyes and molds for all types of material processing, cutting tools, and firearms, optics, watches, thin films (window tints, food packaging, etc.) and in the textile industry [43].

II.4.1.1. Different types of PVD

1. **Cathodic arc deposition**: In which a high-energy electric arc discharges a high-energy electric arc onto the target material (source) some material into a highly ionized vapor to be deposited on the workpiece.

2. Electron beam physical vapor deposition: In which the material is heated the material to be deposited is heated to a high degree of vapor by electron bombardment in a “high” vacuum in a “high” vacuum and is transported by diffusion to be deposited by condensation on the (cooler) work piece.

3. Evaporative deposition: The material to be removed is heated to high vapor pressure by electrical resistive heating electrically resistive heating in a “low” vacuum.

4. Pulsed laser deposition: A high-power laser ablates material from the target into vapor.

5. Spray deposition: Where a glowing plasma is discharged (usually localized around the “target” by a magnet) bombarding the material, spraying some of the material away as vapor for subsequent deposition [44].

II.4.1.2. Pulsed Laser Deposition (PLD)

Pulsed laser deposition (PLD) offers great flexibility for several reasons. With this technology, the energy source is located outside the chamber, allowing the use of ambient gas or ultra-high vacuum (UHV). PLD is a physical vapor deposition method where a high-energy

pulsed laser beam is directed at a target material of the desired composition. The vaporized material then condenses on a substrate placed against the target, forming a thin film. This process can occur either in ultra-high vacuum conditions or in the presence of a background gas, such as oxygen for oxide film deposition. The PLD allows the adjustment of various parameters that significantly affect the properties of the deposited films [45]. Figure II-2 shows a typical PLD setup schematically.

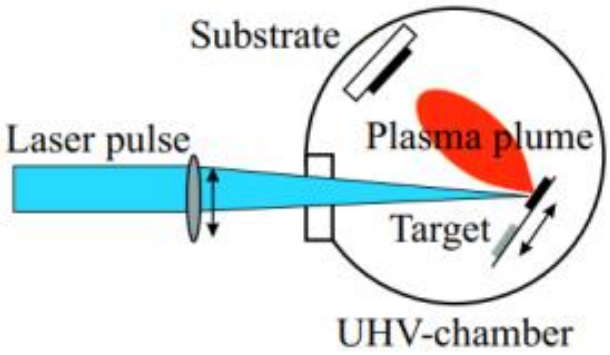

Figure II-2: The pulsed laser deposition (PLD) method [45].

II.4.1.3. II.4.1.3. PVD-Sputtering

The working principle of the PVD-sputtering process in which a substrate is made as anode and the deposition or target material is made as cathodes, which are separated by a distance in the range of 5^{-10} cm in a chamber having vacuum in the range of 10^{-6} to 10^{-10} torr. Flow of an inert gas such as argon (Ar) is continuously provided to the vacuum chamber in which its molecules become positively charged ions ejecting electrons under applied high pressure and voltage. The ejected electrons may further ionize other gas atoms to sustain the glow discharge and create a cascading process until all the gas molecules ionize. These ions strike the cathodic deposition material-ejecting molecules from its surface by transfer of their momentum. This phenomenon is known as sputtering [46].

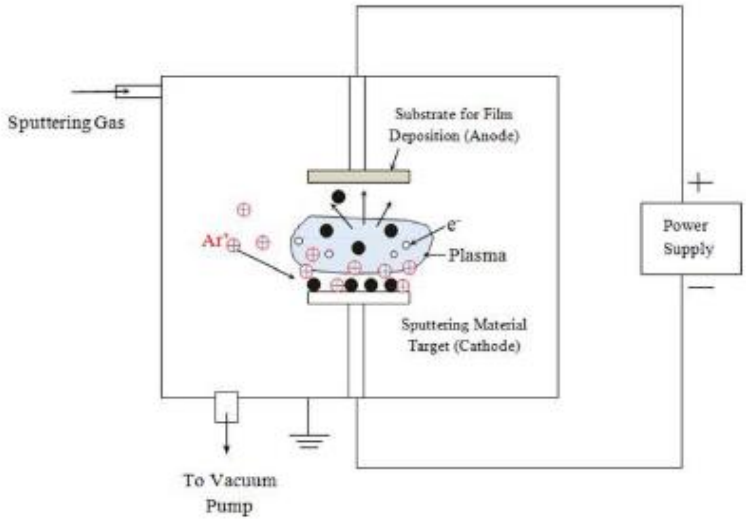

Figure II-3: Working principle of PVD-sputtering process.

II.5. Chemical Processes

II.5.1. Chemical Vapor Deposition (CVD)

Chemical vapor deposition (CVD) is a process in which a gas phase reacts chemically to produce one or more condensed (deposition) phases as well as gaseous product species. The process of laboratory or typical industrial CVD process involves a dynamic flow system in which gaseous reactants pass over a heated substrate. These gases react chemically to produce a condensed coating on the substrate on the substrate as well as the product gases, and then these product gases as well as any remaining reactant gases remaining from the hot reaction zone. A CVD process can be described in terms of systems chemistry (chemical species, thermodynamics dynamics, kinetics, reaction mechanisms), mass transfer (gaseous diffusion, forced convection) and gas flow behavior (flow types, flow patterns, velocities) [47]. Synthesis methods include [48]:

- plasma-enhanced chemical vapor deposition (PECVD).
- atmospheric pressure CVD (AP-CVD).
- low-pressure CVD (LP-CVD).

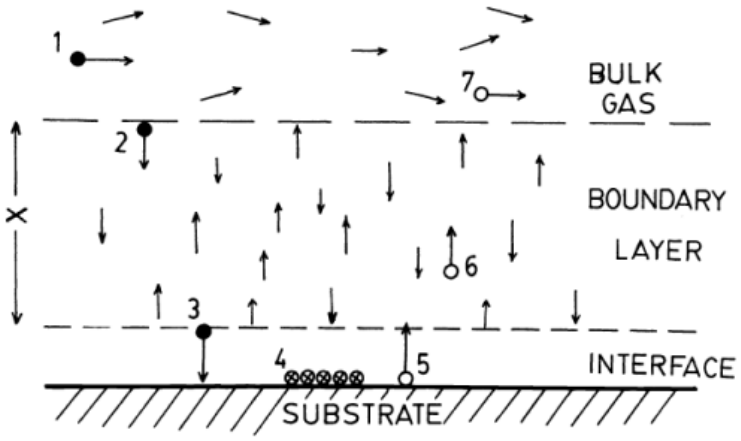

Figure II-4: Schematic Diagram Showing CVD Process [47].

II.5.2. Spray Pyrolysis

A solution of various reactive compounds is sprayed onto a heated substrate using an atomizer. The temperature of the substrate activates the chemical reaction between the compounds. The experiment can be carried out in air, and can be prepared in an enclosure (or reaction chamber) under a vacuum of around 50 Torr [48].

The description of film formation by the Spray pyrolysis method can be summarized as follows:

1- Droplet formation at the nozzle outlet.
2- Decomposition of the precursor solution on the surface of the heated substrate by pyrolysis reaction.

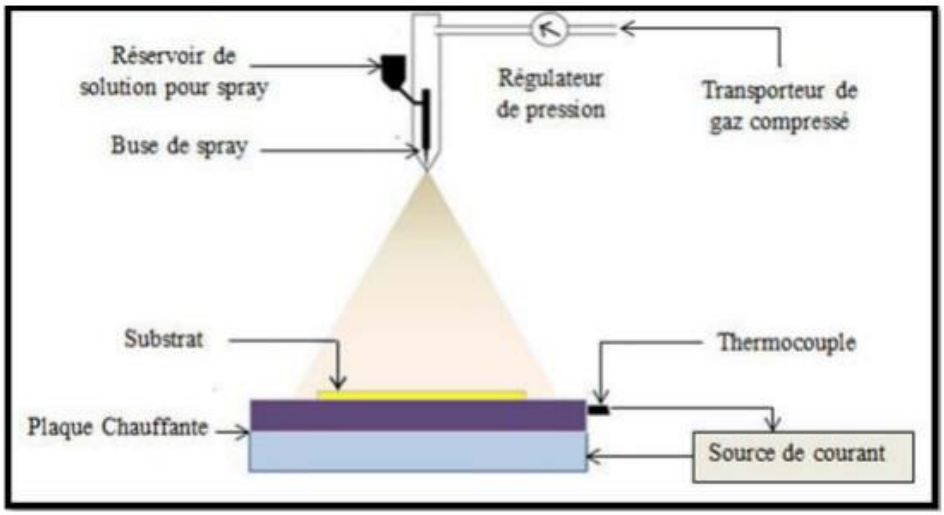

Figure II-5 : General schematic of a spray pyrolysis deposition process [48].

In the remainder of this chapter, we present in detail the sol-gel technique used, which is the spin-coating, it is the technique adopted in this study.

II.5.3. Sol-Gel

At the end of the 1970s, the sol-gel process was developed and widely used in the production of materials with special properties in the chemical and optoelectronic fields.

The name sol-gel is a contraction of the terms “solution-gelification”, and is one of the chemical techniques, that implemented under soft chemistry conditions, with temperatures significantly lower than those required for other conventional synthesis techniques. The synthesis techniques conditions usually provide the opportunity to combine and couple organic and inorganic species to form new families of organic-inorganic hybrid compounds with novel properties. This process can be used in various fields such as encapsulation and the development of hyper-porous materials, but its main application is in the production of thin-film deposits.

II.5.3.1. Principle of the Sol-Gel method

The principle of this technique is to produce a solid material from a liquid solution by chemical reactions at near-ambient temperatures. These mechanisms are based on the transformation of a stable liquid solution (Sol) into a solid material (a dry Gel called xerogel).

solution (Sol) into a solid material (a dry Gel called xerogel) via a process of inorganic polymerization. The time required for the “sol” to transform into a “gel” is called the gel time (or gel point). The process has great potential, as it can produce extremely diverse material forms, from nanoparticles to thin films to large glasses [49].

II.5.3.2. Sol-Gel synthesis

The starting solution (precursor) constituting the “Sol” is a chemical reagent that triggers the reaction.

Precursor routes sol-gel synthesis:

Colloidal or inorganic route: Obtained from metallic salts in aqueous solution (chloride, nitrate, oxychloride, etc.). This cheap route is difficult to control, which is why it is still rarely used. However, it is the preferred way of obtaining ceramic materials.

Polymeric or metal-organic route: This route is made from metal alkoxides in organic solutions.

In both cases, the reaction is initiated by hydrolysis (adding water to the alkoxide route and modifying the pH of the inorganic route to form hydroxides) to form gels composed of particles called hydrogels, whose chemical nature corresponds to a hydrated oxide: MO_X, nH_2O.

II.5.3.3. Reaction mechanisms in the Sol-Gel process

In the sol-gel method, the chemical mechanism usually decomposes in two stages: hydrolysis and condensation. Each gel obtained was linked to the appropriate materials.

Hydrolysis reaction: The hydrolysis of substances is the decomposition by water of H^+ and OH^- ions from the dissolution of water. The result is a nucleophilic substitution of the -OH ligand by the -OR ligand. This reaction is accompanied by the consumption of water and the release of alcohol, namely the hydroxyl group (R-OH) [49,50], as shown in the following reaction:

$$M\text{-}(OR)_n + H_2O \rightarrow HO\text{-}M\text{-}(OR)_{n-1} + R\text{-}OH$$

Its aim is to generate reactive M-OH functions. This involves the conversion of alkoxide functional groups into hydroxyl functional groups. The resulting solution is called sol.

Condensation reaction: The $HO\text{-}M(OR)_{n-1}$ groups generated during hydrolysis react either with each other to give a molecule of water (Reaction 2). Or with a molecule of alkoxide M(-OR) to give a molecule of alcohol (reaction 1), leading to the formation of M-O-M bridges where each oxygen atom becomes a bridge connecting two atoms of metal M. This corresponds to the formation of a gel whose viscosity increases over time. This gel contains solvents and precursors that have not yet reacted [51,52].

This process governs the following reactions at room temperature:

$$(OR)_{n-1} – M–OH + HO–M– (OR)_{n-1} \rightarrow (OR)_{n-1}–M–O–M– (OR)_{n-1} + R–OH$$

$$(OR)_{n-1} – M–OH + HO–M– (OR)_{n-1} \rightarrow (OR)_{n-1}–M–O–M– (OR)_{n-1} + H_2O$$

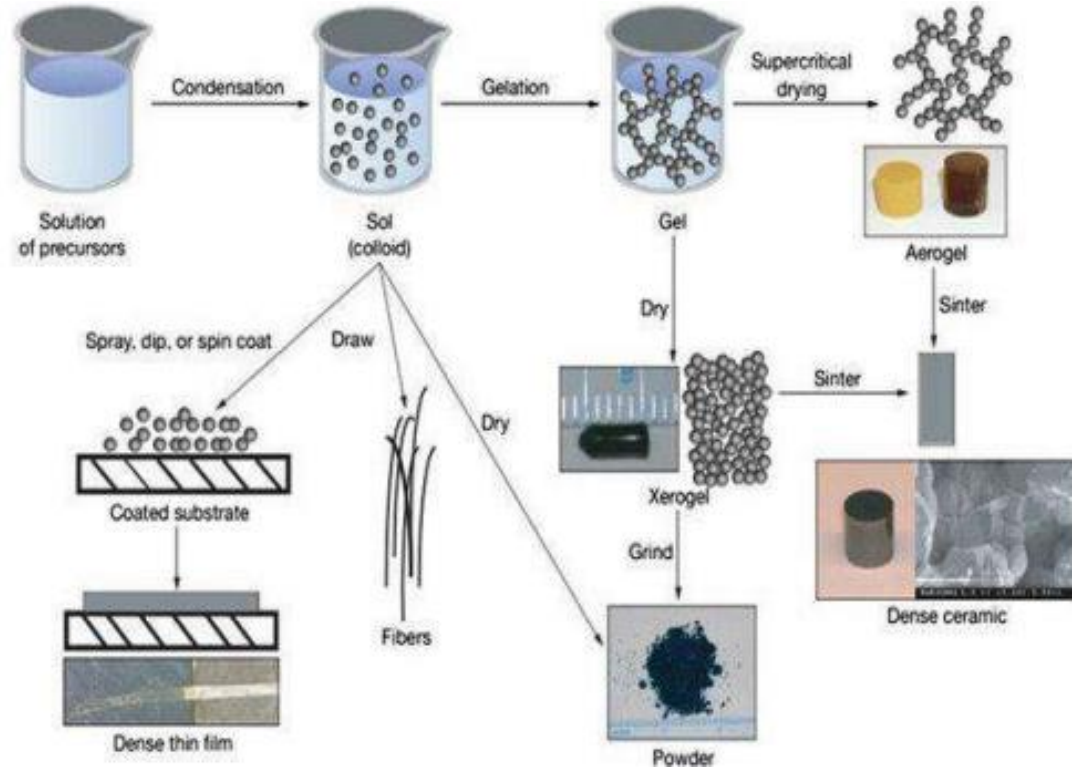

Figure II-6 : The schematic diagram of sol-gel method [53].

Jellification: The preceding reaction leads to gelation of a gel composed of M-OM (or M-OH-M) chains, whose viscosity increases with time. The gel still contains solvent and unreacted precursors. After gelation, the material dries due to capillary forces in the pores, and this drying causes volume shrinkage when alcohol or water evaporates [54].

Ageing: The chemical and physical changes that continue during aging after clotting are significant. During this process, more cross-linking continues, the gel shrinks as covalent bonds replace non-cross-linked bonds, and the pore size and pore wall strength change over time. As covalent bonds replace non-bonding bonds, the pore size and pore wall strength change as the gel structure evolves: Evolution of gel structure [50].

Drying: From the same solution and depending on how the gel is dried, there are several types of drying different types of materials [50] (Figure II-6):

Erogel: conventional drying (normal evaporation) results in a volume reduction of 5 to 10%. In this mode, the residual liquid exerts a very strong capillary force, resulting in reduced microporosity and a dry gel structure.

Aerogel: drying under supercritical conditions (in a high-pressure autoclave) results in little or no volume shrinkage. The gel gives a very open “aerogel” structure with good microporosity.

II.5.3.4. Solution deposition processes

Dip-coating :

This method involves dipping the substrate into the solution and withdrawing it at a constant speed. The principle consists in immersing the substrate in the solution and withdrawing it at a constant, controlled speed to obtain a film of uniform thickness. This system enables high quality films [51]. FigureII-7 shows the three stages of deposition using the dip-coating process.

Soaking, drawing and evaporation of the solvent at room temperature.

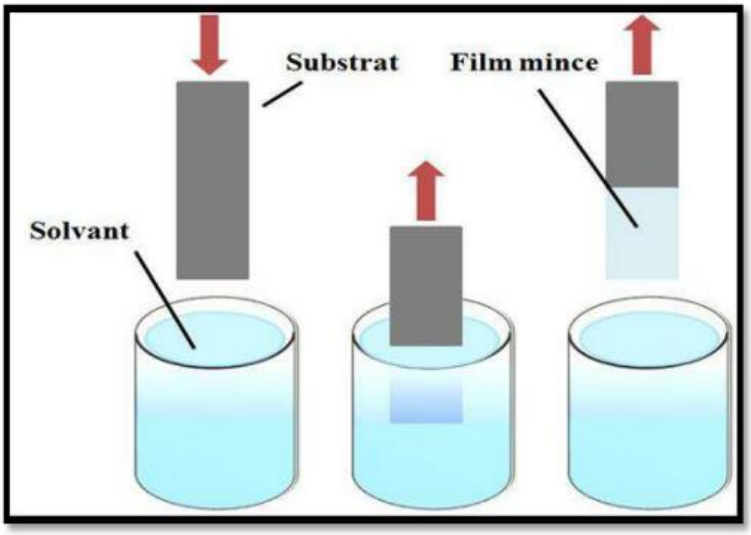

Figure II-7: Dip-coating stages [47].

Spin-coating:

This method involves centrifuging an excess solution onto a substrate. The advantage of this technique is that it is easy to use, and requires little investments. It gives excellent results on flat substrates with dimensions of the order of cm^2. This deposition method can be broken down into four phases [57], as shown in figure II-8:

1) Deposition of the solution.

2) Start of rotation: the acceleration phase causes the liquid to flow out wards the outside of the substrate.

3) Rotation at constant speed ejects excess liquid in the form of droplets and a uniform reduction in film thickness.

4) Evaporation of the most volatile solvents, which further reduces the thickness of the deposited film.

The final film thickness and other properties depend on the nature of the liquid (viscosity, drying rate, solids percentage, surface tension, etc.) and the parameters chosen for the dewatering process. Factors such as final rotational speed, acceleration, and vapor evacuation affect the properties of coated films [58] .

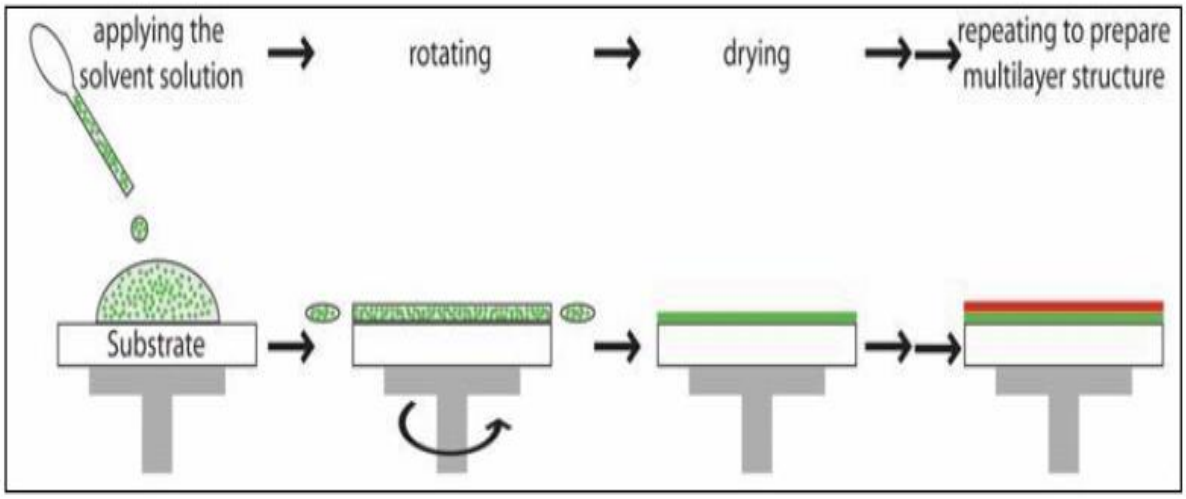

Figure II-8*: four steps of* spin *coating [58]*.

II.5.3.5. The advantages of the Sol-Gel technique

1. Good quality (homogeneity) of thin film.
2. Purity of precursors.
3. Possibility of producing an oxide thin film on a thermosensitive substrate at temperature (low energy cost).
4. multi-component deposition in a single operation.
5. Thin films deposited on both sides of the substrate [59].

II.5.3.6. disadvantages of the Sol-Gel technique

1. Long, complicated process.
2. Handling of large quantities of solvents.
3. High cost of alkoxide precursor.

4. Low layer thickness is the major drawback of this method, as well as the fact that to obtain an epi-pass sample, several layers have to be applied, multiplying the risk of cracking [59].

II.6. Characterization Methods

Once thin films have been produced, a number of characterizations are required to control and optimize the effect of various deposition parameters, such as temperature, humidity and pressure. These characterizations make it possible to control and optimize the effect of several deposition parameters, such as temperature, dopant concentration, flow rate... These layers will be analyzed characterization techniques.

Thin film characterization is based on the following methods:

II.6.1. Thickness Measurements

The thickness “d” is calculated using the gravimetric method [59]:

$$\mathbf{d} = \frac{\mathbf{m}}{\boldsymbol{\rho}.\mathbf{A}} \qquad \textbf{(II-1)}$$

Where:

m: is the mass of the deposited layer (g).

A: is the surface area of the sample (cm^2).

ρ: is the layer density (g/cm^3).

II.6.2. Interference fringe

In a region of high transparency, we observe interference bangs characterized by transmission ripples, as shown in figure II.10. The measurements and analysis techniques are the same.

The physical constants used in the calculations are defined in figure II.9:

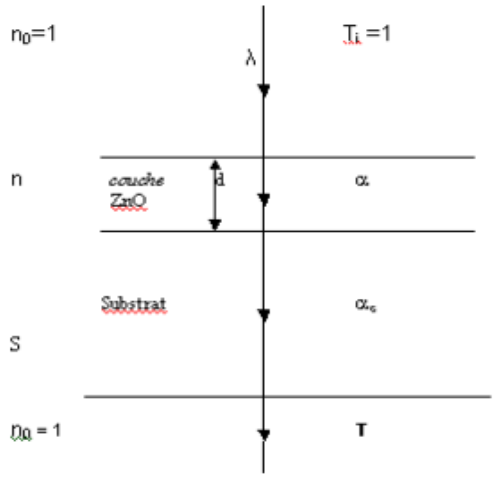

Figure II-9: system of a thin absorbent layer on the thick transparent substrate [60].

T= is the transmission coefficient.

α= is the absorption coefficient of the film.

λ= is the wave length of the incident light.

n and s =are the refractive indices of the film and substrate respectively.

d= is the thickness of the substrate.

Using the physical parameters defined in Figure (II-10), the thickness of the layer can determine from the interference of the fringes. The interference of the fringes appears if the layer is thick and smooth. Multiple reflections between the lower surfaces of the layer, in contact with the substrate, and the free one, this results in interference fringes in the transmission aspect [60], as shown in figure (II-10).

λ_1 and λ_2 are the two the wavelengths of two consecutive maxima correspond to T_{M1} and T_{M2} respectively.

T_m is the transmission of the minima between the two maxima (Figure II-10).

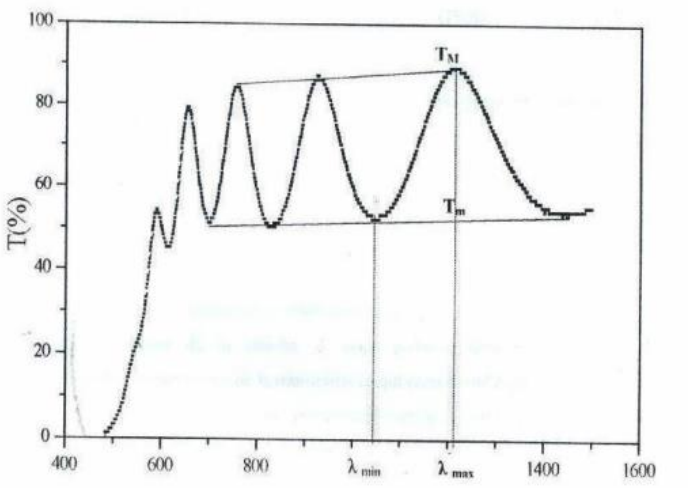

Figure II-10: Interference fringe method for thickness determination [60].

The layer thickness is determined from the relationship:

$$\mathbf{d} = \frac{\lambda_1 \lambda_2}{2(\lambda_1 n_2 - \lambda_2 n_1)} \qquad \textbf{(II-2)}$$

The refractive indices n_1 and n_2 of the layer for wavelengths $\lambda_1$and λ_2 are calculated from the relationship:

$$n_{1,2} = \left[N_{1,2} + (N_{1,2}{}^2 - S^2)^{\frac{1}{2}}\right]^{1/2} \qquad \textbf{(II-3)}$$

S: refractive index of the substrate

and $N_{1,2}$ can be calculated using:

$$\mathbf{N_{1,2}} = \mathbf{2S}.\left[\frac{(T_M - T_m)}{T_M \,.\, T_m}\right] + \left(\frac{s^2 + 1}{2}\right) \qquad (\mathbf{II-4})$$

II.6.3. Structural Characterization

This X-ray diffraction study aims to specify the structure and crystallographic growth directions of the layers, and to measure the lattice parameters and crystallite sizes.II.6.2.1. X-Ray Diffraction

X-ray diffraction is a non-destructive method, which is used to identify the nature and structure of crystallized materials. This method can only be applied to materials crystalline state, i.e. an ordered, periodic arrangement of the atoms orderly and periodic arrangement of their constituent atoms. X-rays, with wavelengths below of less than 1 nm, are used to observe diffraction phenomena in crystals. The method involves bombarding the sample with X-rays, and observing the intensity of the X-rays are scattered according to their orientation in space. The scattered X-rays interfere with each other, so the intensity peaks in certain directions; this is known as “diffraction “phenomenon. The intensity detected is recorded as a function of the beam's angle of deflection 2θ [58]. This is illustrated in Figure II-9.

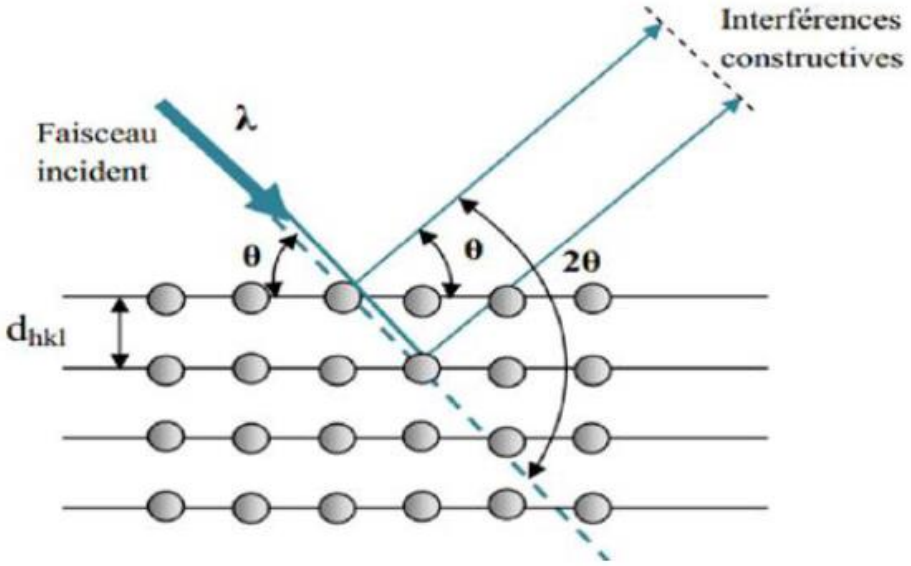

Figure II-11: Bragg diffraction scheme [57].

The directions, in which interference is constructive, called “diffraction peaks”, can be determined very simply by the formula, known as Bragg's law:

$$2d_{hkl} \sin \theta_{hkl} = n\lambda \qquad \textbf{(II-5)}$$

$d_{hkl:}$ Inter-reticular distance, i.e. the distance separating the index planes (hkl).

θ_{hkl}: Angle of incidence of X-rays on the surface of the material under study.

n: Order of reflection (integer number).

λ: X-ray beam wavelength.

Since crystallographic planes can be identified by Miller indices (hkl), we can index diffraction peaks according to these indices, we can index diffraction peaks according to these indices. The advantage of this method is that it allows us to distinguish between different crystallization forms of the same compound. The advantage of this method is that it enables us to distinguish between the different crystallization forms of the same compound.

In fact, this method makes it possible to identify the phases present in the layer and their possible orientations by comparison of the inter-peak distances. Their possible orientations by comparing inter-reticular distances and intensities against reference files drawn up by the Joint Committee for Power Diffraction File (JCPDF). This technique allows us to determine the crystalline state of the thin films obtained, and to provide valuable information on the various compounds and/or phases present. The Figure shows a schematic diagram of the diffractometric setup. Instrument control the instrument is computer-controlled.

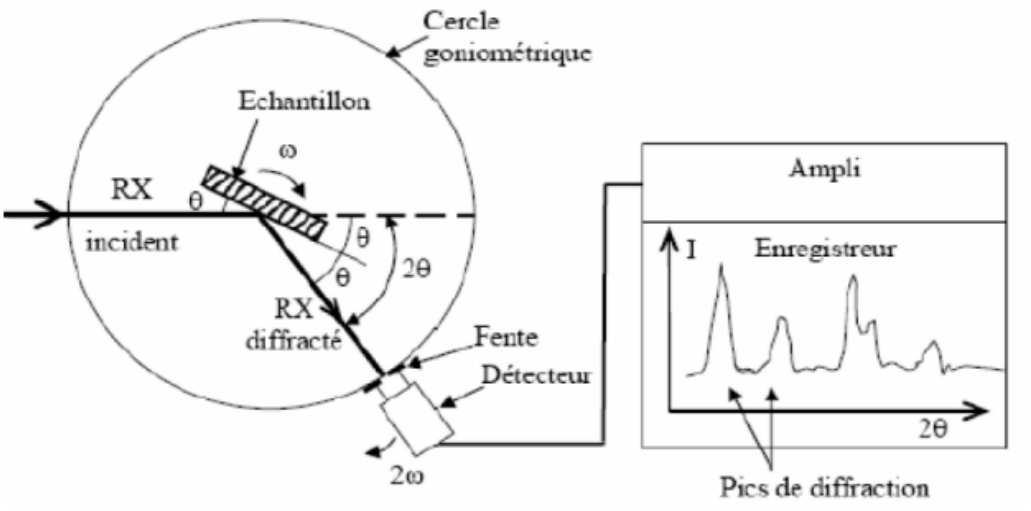

Figure II-12: Schematic diagram of a diffractometer counter [57].

In our study, we used a diffractometer type: "Rigaku Mini Flex 600" (Université Mohamed Khider Biskra); the X-rays were produced from a Cuka radiation source, with a wavelength of 1.541838 A, at an accelerating voltage of 40 kV and a current of 40 mA [58].

Figure II-13: "Rigaku Mini Flex 600"type diffractometer.

The XRD spectrum provides a wealth of information, in particular:

The number of lines gives an indication of whether the material is monocrystalline or polycrystalline,

The fineness of the line provides information on crystalline quality; Peak intensities can be used to identify preferential orientations, by comparing TC (hkl) texture coefficients of the different peaks in each diagram,

Peak positions can be used to identify crystalline phase, mesh parameters, and internal layer stresses. The width at half-height, together with the position, of the peaksenables grain size to be measured, etc. [58].

II.6.4. Mesh Parameters Determination

By recording the spectrum of the sample, we can determine its lattice parameters. According to Bragg's formula, each diffraction angle θ_{hkl} corresponds to a reticular plane (hkl)

and an inter-reticular distance d_{hkl}. These quantities are related to the sample's lattice parameters. The lattice constants (a and c) of both the ZnO and Co_3O_4 phases were calculated according to the equation (II-2) for the hexagonal structure, and the equation (II-7) for the cubic structure [59]:

$$d_{hkl} = \frac{a}{\sqrt{\frac{4}{3}(h^2+k^2+hk)+l^2\frac{a^2}{c^2}}} \quad \textbf{(II-6)}$$

$$d_{hkl} = \frac{a}{\sqrt{(h^2+k^2+l^2)}} \quad \textbf{(II-7)}$$

where:

d_{hkl}: interreticular distance.

c, a: crystal parameter.

(hkl): Miller indices.

In (002) peak we determine the parameter c:

$$c = \frac{\lambda}{\sin\theta_{(002)}} \qquad (II-8)$$

Using Bragg's law (II-2) in (100) peak we determine the parameter *a* [59]:

$$a = \frac{\lambda}{\sqrt{3}\sin\theta_{(100)}} \qquad (II-9)$$

II.6.5. Crystallite Size Determination

And another parameter that can be determined with the help of diffraction spectra.by measuring the full width at half maximum (FWHM) of the most intense peaks, we can then the average crystallite size "D" can be estimated using Scherrer's formula [60]:

$$D = \frac{0.9.\lambda}{\beta\cos\theta_{hkl}} \quad \textbf{(II-10)}$$

Where:

D: Grain size in Å or nm;

λ: X-ray beam wavelength.

θ_{hkl}: diffraction angle.

β: Half-height width of the most radiantly intense peaks.

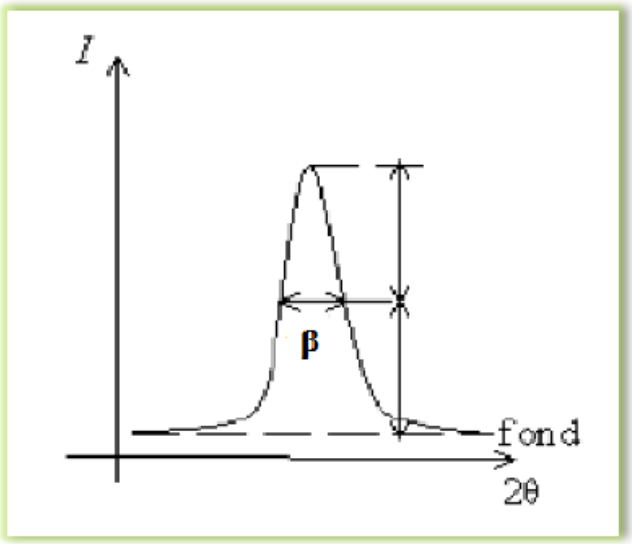

Figure II-14: The definition of β from the X-ray diffraction pic [60].

The use of Scherrer's formula assumes that the profile of diffraction peaks only results from the effects of the apparent size of its crystals and the geometry of the diffractometer. The effects of its apparent crystal size and the geometry of the diffractometer [60].

From the grain size we can calculate the dislocation density using the following formula: $\delta=1/D^2$

II.6.6. Strain Determination

Constraints are internal forces in matter. The relationship between stresses (σ_{ij}), strain tensors (ε_{ij}), and elasticity constants (C_{ij}) is given by the following law:

$$\boldsymbol{\sigma_{ij} = C_{ij}.\varepsilon_{ij}} \qquad \textbf{(II-11)}$$

To calculate these stresses, it is necessary to have the values of the elasticity constants, but these are not always available in the literature (as in the case of ZnS), and as long as strain

varies proportionally with stress, we can use this relationship between these two variables to get an idea of the stress variation in the of the layers studied, using the strain (ε) formulas follows [60].

$$\varepsilon = \frac{\beta \cos\theta}{4} \qquad \textbf{(II-12)}$$

II.7. Optical Characterization

We used UV-Vis spectroscopy, which enabled us to measure curves representing the variation in transmittance as a function of wavelength. By exploiting these curves, we can estimate the thickness of the film and determine its optical properties such as optical absorption edge, absorption coefficient, band gap width, and Auerbach energy.

II.7.1. Spectroscopy UV-Visible

The operating principle of the UV-VIS-NIR spectrophotometer is shown in the following figure (II-14):

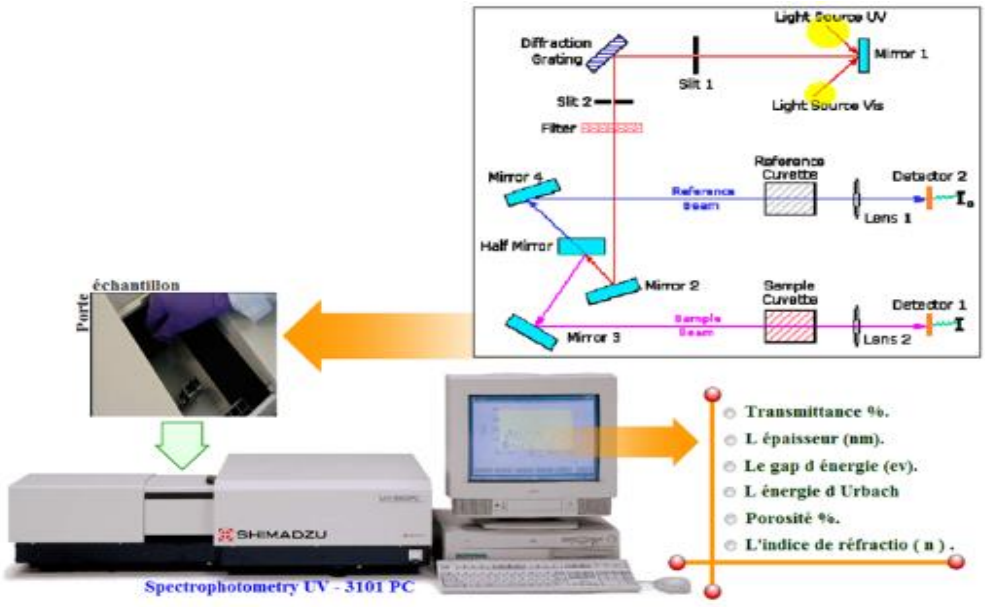

Figure II-15: Schematic representation of the spectrophotometer [61].

II.7.2. Transmittance Spectra

The transmission coefficient, or transmittance T, is defined as the ratio of transmitted light intensity to incident light intensity [62].

It is calculated directly from the following equation [63]:

$$T = (1 - R)\exp^{-\alpha d} \quad \textbf{(II-13)}$$

Given α as the absorption coefficient of the material, when we contemplate a homogeneous material with a thickness of d and subject it to normal incidence, the amount of light transmitted or transmittance (T), represented as a percentage, is defined as follows [62]:

$$T = \frac{I}{I_0} \times 100 \quad \textbf{(II-14)}$$

where:

the light transmitted at the output is written according to the Beer-Lambert law [63]:

$$I = I_0 \ \exp^{-\alpha.d} \quad \textbf{(II-15)}$$

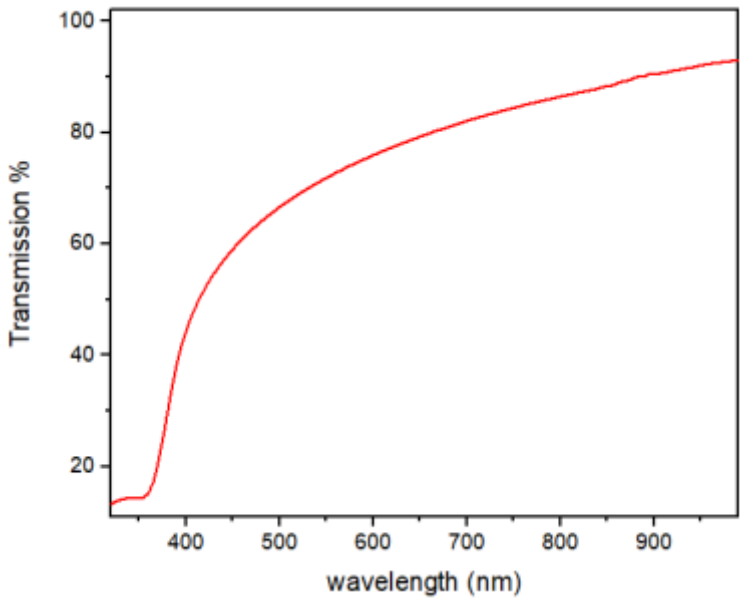

Figure II-16: The transmittance spectrum as a function of wavelength.

II.7.3. Optical Band Gap

The gap energy is determined by the Tauc formula:

$$(\alpha \nu h)^2 = A'(h.\upsilon - Eg) \quad \textbf{(II-16)}$$

Where:

α: absorption coefficient (cm^{-1}).

h: Planck's constant (J s).

hν: Photon energy (J).

A': Constant.

Eg: Gap energy (eV).

The extrapolation to the x-axis (αhν = 0) of the linear part of the curve $(\alpha h\upsilon)^2$ as a function of *hν*, we can deduce the gap energy (Eg) [64], as shown in Figure II.15:

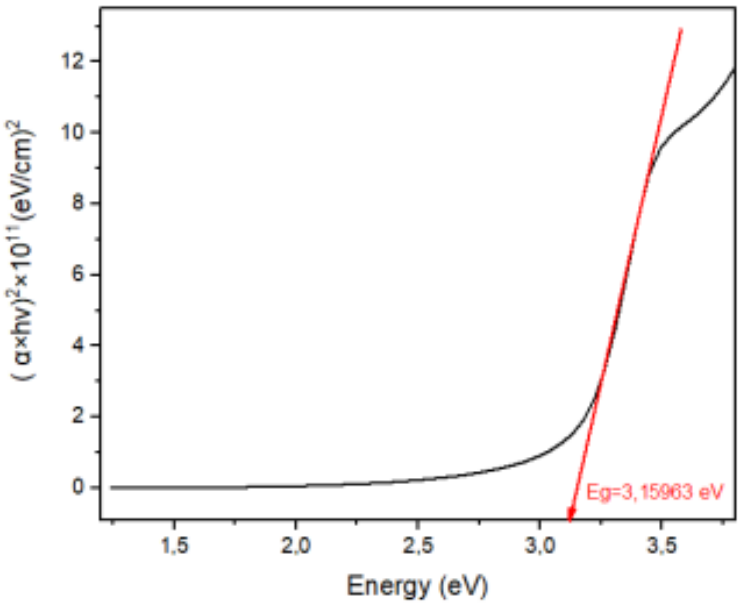

Figure II-17: Gap energy determination [65].

II.7.4. Urbach Energy

Another important parameter characterizing material disorder is Urbach's energy. According to Urbach's law, the expression for the absorption coefficient is of the form [66]:

$$\alpha = \alpha_0 \exp\left(\frac{h\upsilon}{E_{00}}\right) \quad \textbf{(II-17)}$$

By plotting ln(α) as a function of hυ, we can determine the value of E_{00}:

$$\ln\alpha = \ln\alpha_0 + \frac{h\upsilon}{E_{00}} \quad \textbf{(II-18)}$$

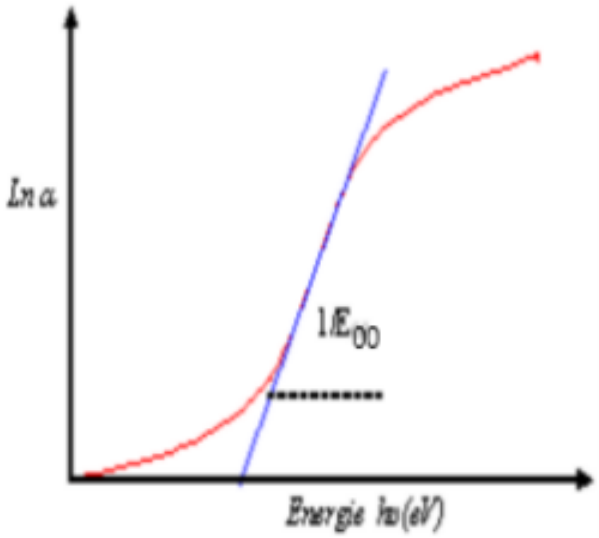

Figure II-18: Determine the turbulence by extrapolating from the variation of ln(α) as a function of hν for a thin layer [67].

II.8. Electrical Characterization

Electrical characterization is one of the most powerful techniques in existence for material characterization. Basic electrical characterization of semiconducting thin films includes determining the conductivity, kinetics, and carrier concentration of the films. The conductivity (or resistance) of the films was investigated using the four-probe technique.

II.8.1. Four-Points Probes Method

Four-point probe measurements are utilized for determining the specific resistance of either a bulk or thin sample. Through employing a four-probe arrangement, the measured resistivity exclusively pertains to the specimen itself, devoid of any influence from the contact point as observed in a two-electrode setup. The configuration for a four-probe measurement is depicted in Figure II.17. Here, a current (I) is conducted through the sample, while the voltage (V) is gauged, as illustrated in the figure. Subsequently, the specific resistance of the sample can be computed. Such computations necessitate certain assumptions. Namely, it is assumed that the metal tip is infinitesimally small, and the samples possess almost infinitesimal lateral

dimensions. This holds particularly true for bulk samples wherein the thickness (t) significantly surpasses the lateral dimensions [68].

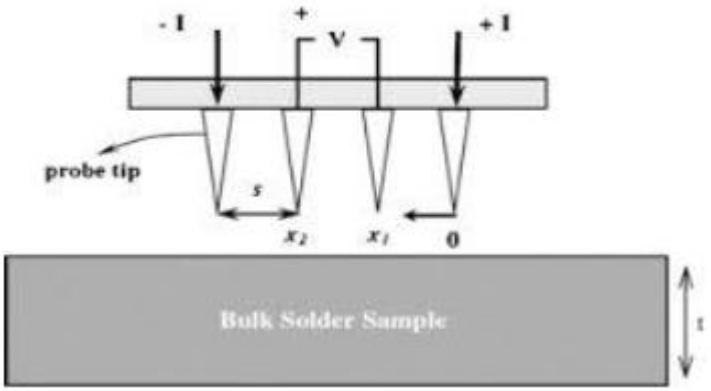

Figure II-19: Schematic of four-point probe configuration [68].

II.8.2. Electrical Resistivity Measurement

The electrical resistivity of films deposited on quartz substrates is measured at room temperature using the four-point method (Jandel system). The configuration used is illustrated in Figure II.17. During measurements, the four metal probes points are brought into contact with the sample surface. A current source passes through the two external probes, a voltmeter measures the voltage V across the two internal probes. The distance between the probes is 1 mm. The current source is a Keithley 237 generator, and the voltage is measured with a Keithley 2700 multimeter. Film resistance is derived from formula (II.16). The average value of five measurements were taken into account [69].

$$R_s = 4.532 \times \frac{V}{I} \qquad \textbf{(II-19)}$$

Where 4.532 is a form factor specific to thin film measurement, V: measured voltage between probes 2 and 3 (V), I: current applied between 1 and 4 probes (A).Knowing the film thickness d, its resistivity can be obtained from the following equation [69]:

$$\rho = R_s \cdot d \qquad \textbf{(II-20)}$$

From the resistivity of the film, we can calculate its conductivity using the formula below.

The electrical conductivity is the inverse of resistivity and is expressed in $(\Omega.cm)^{-1}$.

$$\sigma = \frac{1}{\rho} \quad \textbf{(II-21)}$$

II.8.3. The IV measurement technique for diodes

Diodes are two-terminal electronic devices that typically enable current to flow in one direction (forward bias) and block the current from flowing (reverse bias) in the opposite direction. However, there are many types of diodes that perform various functions, each of these specific types of diodes can be differentiated by their current-voltage (I-V) characteristics. I-V testing of diodes is performed in research labs as well as in a production environment on packaged devices or on a wafer [70].

I-V characterization of a diode typically requires a sensitive ammeter, voltmeter, voltage source, and current source. Being able to program, synchronize, and connect all these separate instruments can be cumbersome and time consuming, as well as require a considerable amount of rack or bench space. To simplify testing and reduce rack space, a single unit, such as B 1500 A Semiconductor Instrument, is ideal for diode characterization because it can source and measure both current and voltage. The Model B 1500 A Semiconductor can sweep the source voltage and measure current over many decades (10–11A to 1A), which is required for diode testing. These measurements can be generated automatically over the bus or just as easily via the large touchscreen, which enables the user to set up tests and graph them on the screen. The Model B 1500 A Semiconductor is pictured in Figure 18 sourcing voltage and measuring current on a LED that is connected to its inputs in a four-wire configuration [70].

Figure II-20:B 1500 A Semiconductor Device Analyzes the I-V characteristics of Diode.

The application note explains how to perform I-V characterization on diodes easily using the Model B 1500 A Semiconductor Device Analyzes. In particular, it describes how to take, graph, and store measurements using the front panel user interface, as well as how to automate the measurements over the bus.

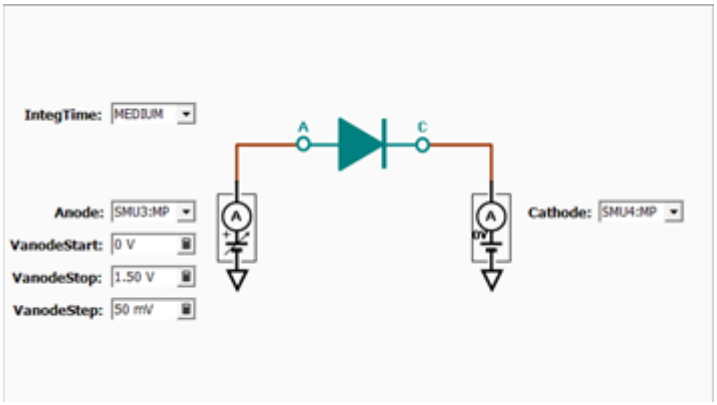

Figure II-21: Junction IV Diode measures the forward and reverse bias anode voltage vs anode and cathode current characteristics.

The thermionic current-voltage relationship of a Schottky barrier diode, neglecting series and shunt resistance [71], is given by:

$$\mathbf{I = I_s\left(e^{(\alpha v)-1}\right)} \qquad \mathbf{(II-22)}$$

Where:

Is = the saturation current.

α=q/nKT with n the ideality factor.

KT/q = 25.10^{-3} V at T=300K.

When series resistances are considered the equation (20) becomes:

$$\mathbf{I = I_s\left(e^{(\alpha(v-R_sI)-1}\right)} \qquad \mathbf{(II-23)}$$

The ideality factor n incorporates all unknown effects making the device nonlinear when greater to unity. Data plotted as Log (I) versus V are linear when V>>KT/q.

In the conventional I-V method, the saturation current (Is) is determined by an extrapolation of the Ln(I) versus V curve to V = 0. The Ln(I) axis intercept for the straight-line portion of this semi log plot at V = 0 is given by ln (Is).

The deviation of the I-V curve from linearity for high voltages is ΔV = IRs, allowing Rs to be determined according to Rs = ΔV/ΔI. When Rs and Is are determined, we can easily obtain n value.

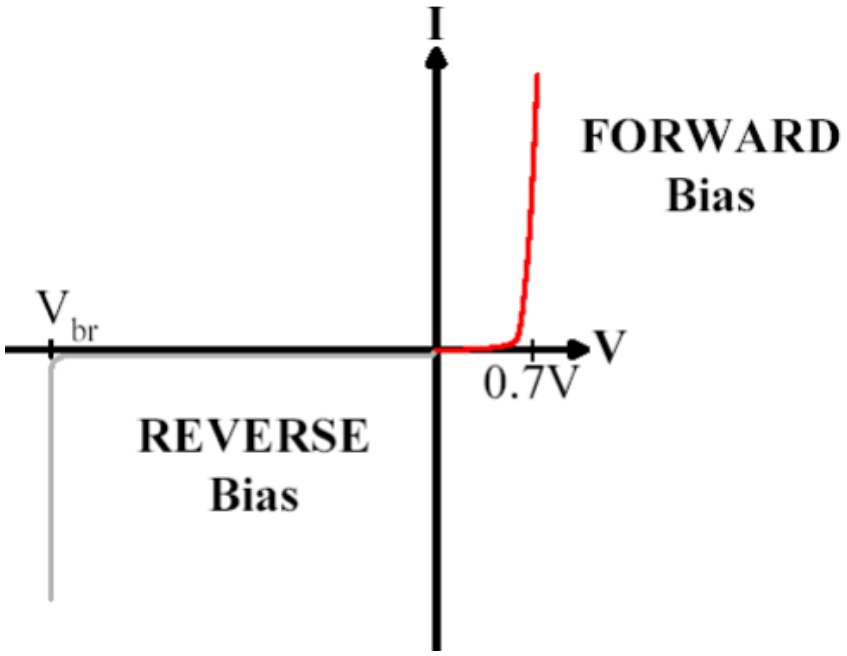

Figure II-22: An ideal diode I-V characteristics [72].

Once the saturation current has been calculated, the barrier height can be estimated in both electrodes in dark and light [4] , from the following:

$$\Phi_{B1} = \frac{KT}{q} ln\left(\frac{A A^{*} T^{2}}{I_s}\right) \quad \text{(II-24)}$$

A the Schottky contact area is 0.031 cm^2 for Ag. A*: is the Richardson constant, A* = 32 A cm^{-2} K^{-2} and T the temperature in Kelvin.

Chapter III: Experimental part: elaboration, results and discussion.

Introduction

The first part of this chapter presents the different steps followed to elaborate ZnO thin films pure, doped with Ga and co-doped with In-Al. the results obtained have been used in manufacturing a ZnO based Schottky diode. The method adopted in this study is gel sol (spin coating). Our work was carried out in Laboratory of Metallic and Semiconducting Materials (LMSM) at University of Biskra in Algeria.

The second part discusses the structural, optical and electrical characterization of samples with different coatings using X-ray diffractometer (XRD), UV-vis spectrophotometer, four-point technique and the I-V measurement technique for diodes to identification of films with optimal properties.

III.1. Used apparatus (Spin coater)

The figure below presents the spin coater devise which used to deposit the ZnO thin films. It has been fabricated in MSML laboratory.

Figure III-1: Spin coater.

III.2. Elaboration of ZnO Thin Films

III.2.1. Choice of deposition substrate

The choice of substrate is linked to the nature of the desired application. Some applications require the use of insulating substrates such as glass. While others require conductive substrates such as ITO In our work, we have used the two types of substrates:

- Glass which constitutes the amorphous and non-conductive material.
- ITO (tin-doped indium oxide) because we noticed that better films are obtained on this crystalline substrate and to use it in ZnO Schottky elaboration.

Indium–tin–oxide (ITO) thin films have been studied extensively in the optoelectronic industry because they combine unique transparent and conducting properties. ITO thin film is a highly degenerate n-type semiconductor which has a low electrical resistivity of $2 – 4\times10^{-4}$ Ω.cm. The low resistivity value of ITO films is due to a high carrier concentration because the Fermi level (E_F) is located above the con-duction level (E_C). The degeneracy is caused by both oxygen vacancies and substitutional tin dopants created during film deposition. The carrier concentration of high conductivity ITO films is in the range of $10^{20} – 10^{21}$ cm^3. Furthermore, ITO is a wide band gap semiconductor (Eg: 3.5– 4.3 eV), which shows high transmission in the visible and near-IR regions of the electromagnetic spectrum [73].

Due to these unique properties, ITO has been used in a wide range of applications. For

example, ITO films are used as transparent electrodes in flat panel displays and solar cells,

surface heaters for automobile windows, camera lenses and mirrors as well as transparent heat reflecting window material for buildings, lamps, and solar collectors [74].

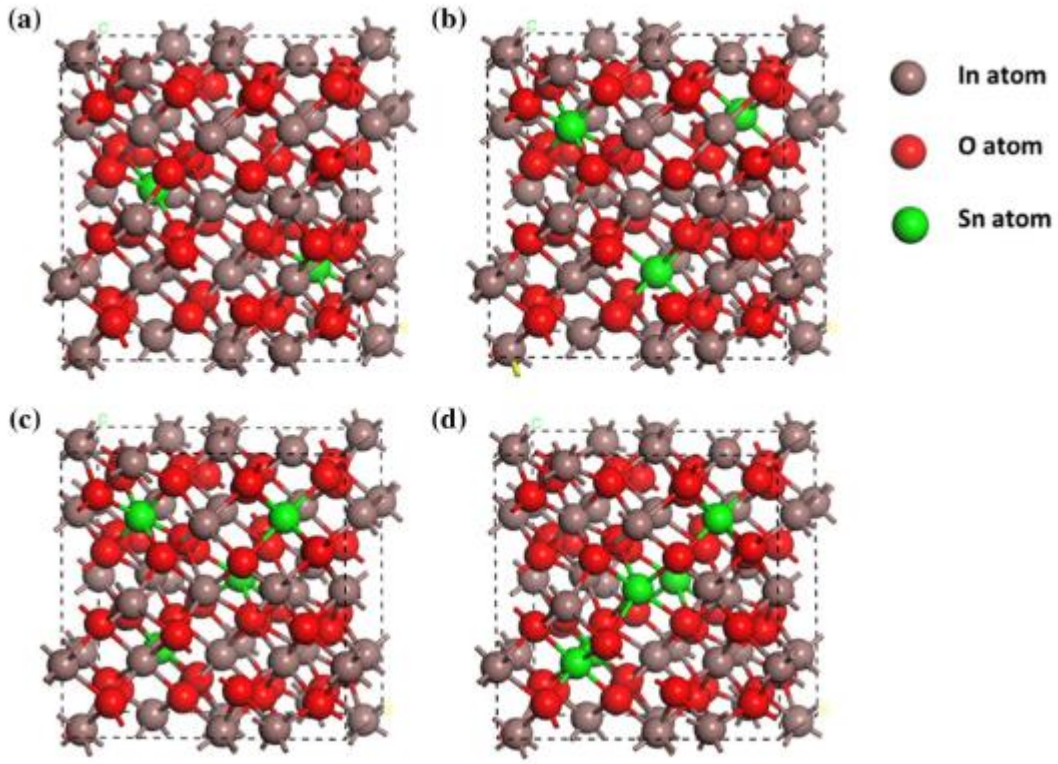

Figure *III-2*:The crystal structure of ITO materials with different Sn-doping concentration **a)** In_2O_3–2Sn, **b)** In_2O_3–3Sn, **c)** In_2O_3–4Sn, **d)** In_2O_3–5Sn [75].

III.2.2. Cleaning of the substrates

The adherence and the quality of the depot repose on purity and the state of the substrate thus the cleaning of the latter is one of the most important steps, the cleaning of our substrates surfaces is as follows:

- The substrates are cut using a pen with diamond point.
- Cleaning with soap solution.
- Rinsing with the water distilled and then with acetone during 5 min.
- Rinsing with distilled water.
- Rising with methanol during 5 min at ambient temperature.
- Cleaning with water distilled in ultrasonic bath.
- Drying using a drier.

III.2.3. Deposition of Thin Film

In all samples, the master solution containing zinc acetate dihydrate solution (Zn (CH3COO)$_2$-2H2O), it was used as a precursor, Absolute ethanol (C_2H_5-OH) and diethanolamine (HN(CH_2CH_2OH)$_2$, DEA) were used as solvent and stabilizing agents. with a molar concentration of the solution is 0.5 M, and the molar ratio of DEA with the acetate was maintained at unity. Aluminum and indium and Gallium were added in the form of nitrates Al (NO_3)$_3$-9H_2O and In (NO_3)$_3$-H_2O, and Ga (NO_3)$_3$. The dopants were dissolved in ethanol to obtain solutions with molar ratios equivalent to 8 at. % for gallium and 4 at. % for (aluminum + indium),The co-doped films were prepared as ZnO:(In 2% + Al 2%). This solution was stirred for 30 min at 60°C temperature to become homogenous. Then it was left to rest for 24 h before thin film deposition in a spin-coating system. The layer was deposited by spin coating at a rotation speed of 1000 rpm for 30sc. After spin coating, each layer was immediately treated thermally at 500°C in oven air for 30 min before spinning the next layer. Each film was obtained through repeated layer deposition times. Each finished film was again treated thermally at 500°C for 30 min in air. The preparation of ZnO thin films is shown in figure III.3.

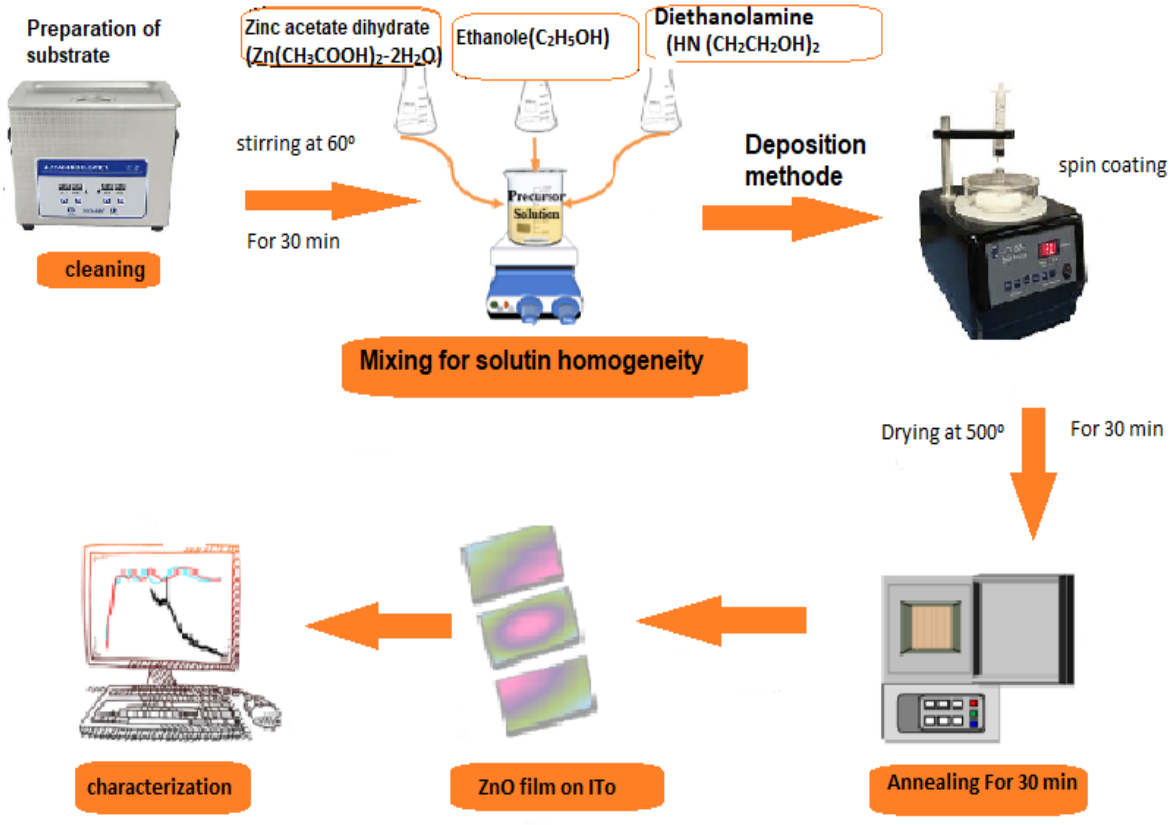

Figure III-3: Schematic represents the experimental procedure.

III.3. Results and discussion

III.3.1. Adhesion test

The adhesion strength between deposited thin films and their substrates can be evaluated in a variety of ways. This test frequently happens before applying any characterization, and in this study, it was specifically evaluated on the thin films applied with Scotch adhesive tape. The degree of adherence is considered "good" if the thin film adheres to the substrate (figure III.4)

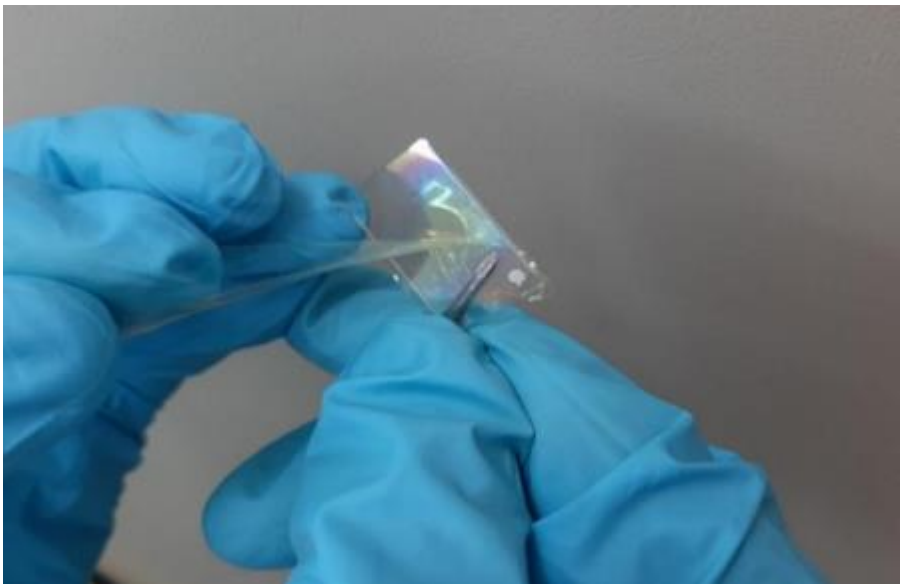

Figure III-4: Simple adhesive tape test for our ZnO thin films.

III.3.2. Structural Properties

III.3.2.1. X-ray Diffraction Spectrum (XRD)

X-ray diffraction results were obtained using the device "Rigaku Mini Flex 600"(Thin films and their applications Laboratory-Biskra), using CuKα radiation with a 1,541874Å-wavelength where all the samples were scanned from 20° to 80°. Figure (III-5), represents X-ray diffractograms of ZnO films with different doping solutions deposited on ITO substrates. The comparison with JCPDS Card No. 01-075-0576 indicates that ZnO films crystallized into the hexagonal wurtzite crystal structure.

The XRD patterns of the ZnO thin films pure, doped and co-doped are displayed in Figure III-5. The presence of several major peaks (100), (002), (101) in the XRD spectra shows that all the films are polycrystalline in nature. In addition of the three main peaks of

zinc oxide, there are three other peaks appeared at 2θ: 47.7°, 56.7°, 63°and 68° which are correspond to (102), (110), (103), and (200) respectively.

While the five additional peaks noticed correspond to the ITO substrate, they are marked by (*). And identify by comparison with JCPDS Card No. 01-089-4598) [76].

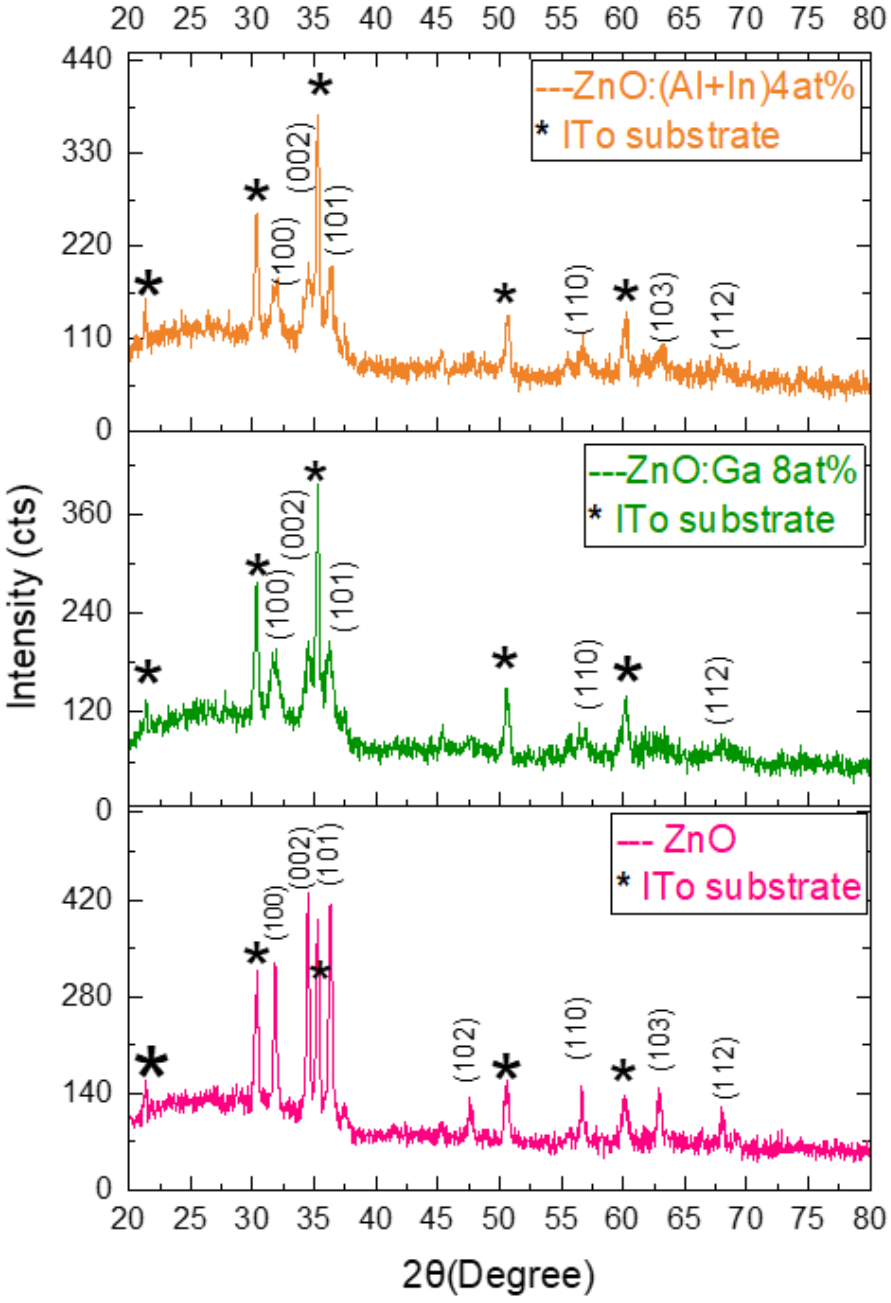

Figure III-5: Spectra XRd of ZnO thin films with different solution**.**

The intensity of the peaks varies among the samples, suggesting differences in crystallinity and possibly grain size. Pure ZnO and ZnO doped with Ga exhibit relatively high peak intensities, implying better crystalline quality compared to ZnO doped with Al and In.

All samples maintain the hexagonal wurtzite structure of ZnO, indicating that doping with Ga, Al, and In does not fundamentally change the crystal structure.

III.3.2.2. Crystallite Size and Strain

The size of the crystallites and the strain were calculated from the width at half maximum (FWHM) of the most intense, using Scherrer's formula. Table III.1 summarizes the corresponding values for crystallite size, strain, and lattice parameters for all the samples.

	2θ (°) (hkl)	B (Rd)	Crystallite Size (nm)	D_{moy} (nm)	ε_{moy}	δ_{moy} (nm^{1})	d_{hkl} (nm)	a (nm)	C (nm)
ZnO Pure	31.855 (100)	0.004	32.340	37.071	7.666 $\times 10^{-4}$	6.333× 10^{-4}	2.809		5.199
	34.497 (002)	0.003	36.720				2.813	3.245	
	36.289 (101)	0.002	51.153				2.807		
Ga-ZnO Doped	31.755 (100)	0.025	51.766	37.875	1.366 $\times 10^{-3}$	3.101 $\times 10^{-3}$	2.599	3.249	5.199
	34.500 (002)	0.012	10.707				2.599		
	36.220 (101)	0.006	51.153				2.602		
Al, In ZnO	31.876 (100)	0.010	12.937	19.973	1.666 $\times 10^{-3}$	2.833 ×10-3	2.475	3.241	5.205

Co-doped	34.458 (002)	0.006	21.420				2.480		
	36.401 (101)	0.005	25.563				2.468		

Table III -1: Structural parameters values of ZnO thin films.

The calculated lattice constants C and a of ZnO thin films (Table III-1) seems to be close to the lattice constant of bulk ZnO (C_0 = 5.206 Å, a_0 = 3.249 Å), The little differences point out the deformation of the unit cell, and it be can explain by the presence of defects and lattice distortions in the crystal.

Also, we have noted that d_{hkl} values are different from the reference (d_{hkl} = 2,603 Å); this variation of d_{hkl} gives rise to the shift of the peaks' position, which is probably caused by the manifestation of the strain during the growth of the films.

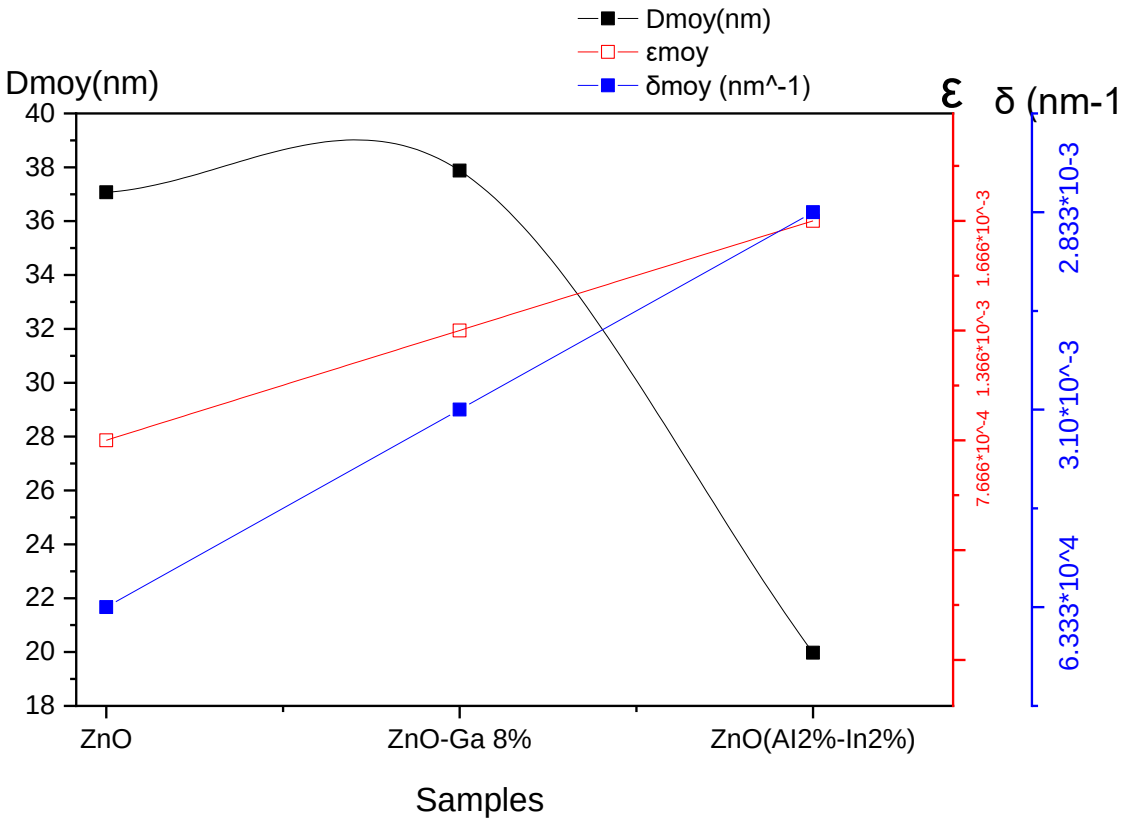

Figure III-6: Crystallite size, strain, and dislocation density as a function of the samples.

The figure (III-6) shows the variation of the grain size for ZnO pure, doped with Ga8% and ZnO co-doped with (Al4%, In4%). The size of the crystals ranges from about 19.973 nm to 37.875 nm. This indicates that the films elaborated are in nanoscale. The larger crystals that registered for ZnO pure (37.875 nm) indicate films are typically more stable and have better electronic properties compared to smaller crystals.

The average crystallite sizes for doped ZnO thin films are smaller than the undoped ZnO; this can be related to the Zener pinning effect, which prevents grain boundary movement and defects in the crystal matrix and acts as a retarding force that slows the formation of crystallites. The doping elements situate in the Zn and O vacancies and interstitial sites, and act as defects that prevent the crystallite ZnO synthesis [77, 78].

The minimum grain size has been registered for Al-In co-doped ZnO thin film (19,973 nm), it can be explained by the difference in the ratio of the doping which is 8% for Ga, and (2% Al, 2% In) and the difference between the atom radius of Ga, In and Al as shown in the table below:

Table III-1 : Atomic and ionic radii of ZnO pure and doped elements [79]

Al / Al^{+3} (A°)	In / In^{+3}(A°)	Ga / Ga^{+3}(A°)	Zn / Zn^{+2}(A°)	O / O^{-2}(A°)
0,53 / 1,43	0,80 / 1,67	0,62 / 1, 53	1,37 / 0,74	0,73 / 1,43

On the other hand, analysis of the relationship between strain (ε) and dislocation (δ), reveals that all doped samples have higher ε and δ values than the undoped ZnO sample, this result confirms the presence of defects in the ZnO crystal as it has been explain .

III.3.3. Optical properties

III.3.3.1. Transmittance

In this work it has been used the EVOLUTION 220 UV-VIS spectrophotometer for ultraviolet and visible light. In the wavelength from 350 to 1200 nm, the transmittance spectra of ZnO thin films deposited with different doping elements and for the diode have been recorded in Figure III-7.

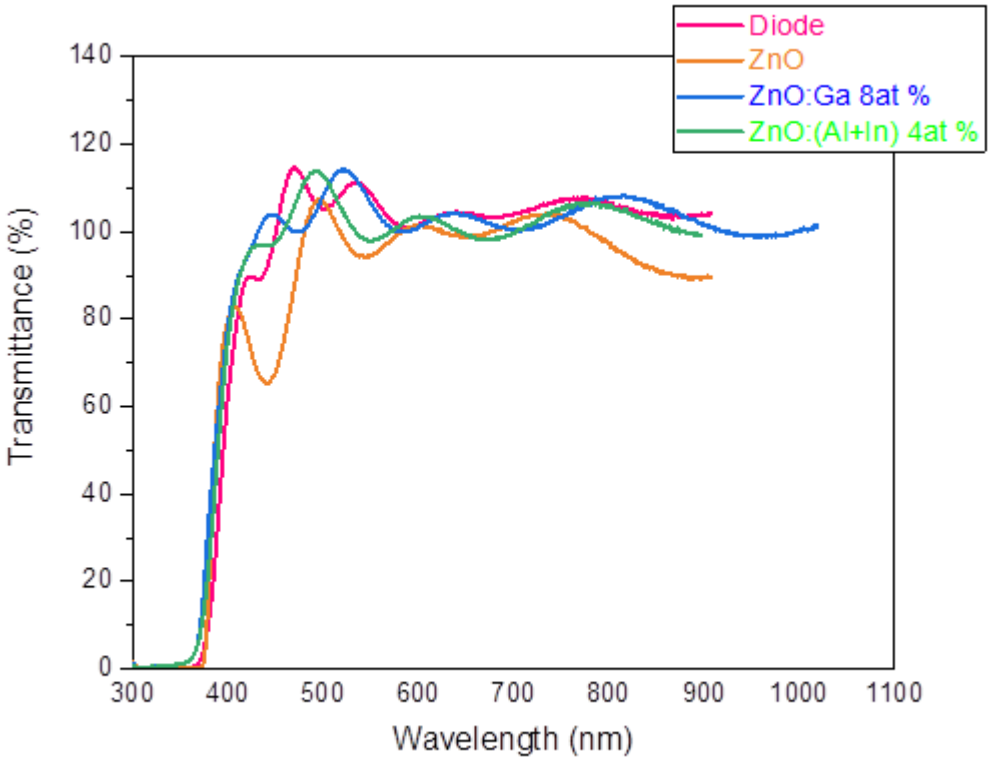

Figure III-7:Optical Transmission Spectra of ZnO Thin Films Deposited with Different samples.

The figure (III-7) presents the transmittance spectra of the films have been deposited on ITO substrate after 24 hours from the preparation of the solution. The spectra show that all the films and the diode have a high transparency (>90%) in the visible region, and high absorption (almost 100%) in the UV region. The transmittance decreases slightly with different doping elements. The same observation has been reported in previous works [78].

It is noted the presence of the interference fringes in all spectra, which confirms the smoothing of all films and the high crystalline quality of the prepared films. The appearance of the fringes permits to calculate the thickness using the Swanepoel method, and this was the main reason why the gravimetric method was chosen to measure the thickness. The low absorption of ZnO thin films in the visible range of the spectrum (~9%) makes these films suitable as a window layer in a Schottky diode as it is confirmed in the diode transmittance specter.

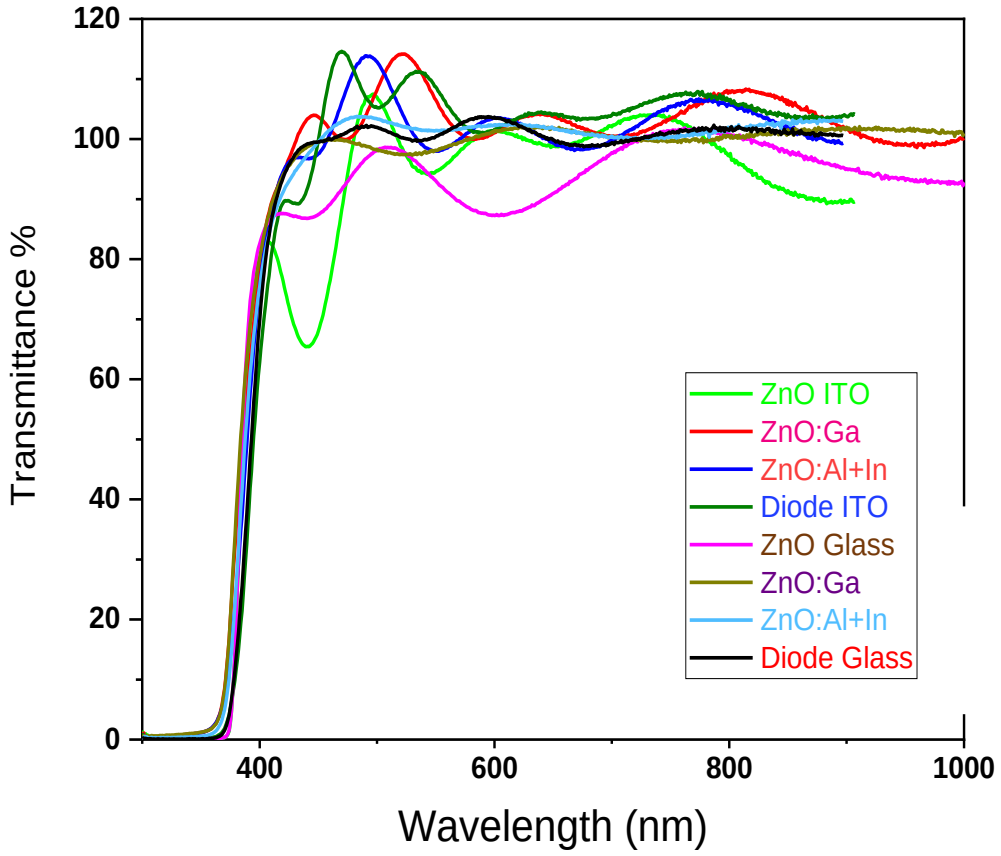

Figure III-8: Optical Transmission Spectra of ZnO Thin Films Deposited with Different samples in a ITO and Glass substrate.

The figure (III-8) is a comparison between the films and diode deposited on glass substrate and the ITO substrate.

It notices that the two substrates' films show a high transmittance, and the choice between is correspond to the uses of the films.

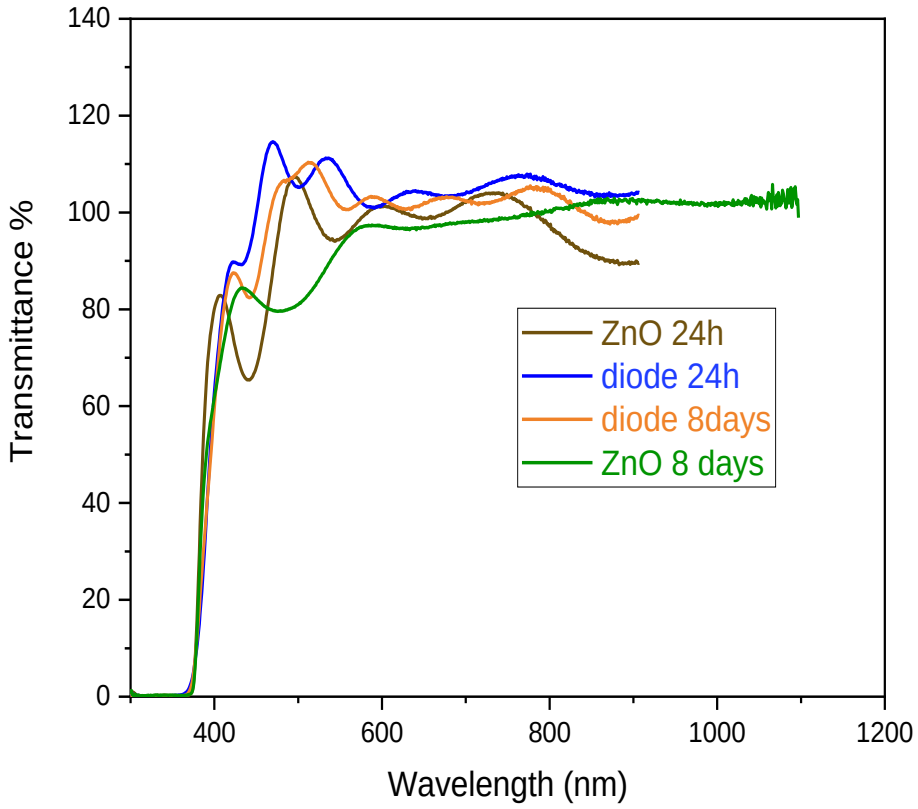

Figure III-9:Optical Transmission Spectra of ZnO Thin Films Deposited with Different samples in effect gel time.

From the restriction of the preparation conditions which cause the solutions to age, we used this point to compare between the transmission of the solution used after 24 hours and the old solution (Figure III-9). It has notice that ZnO thin films shows some degradation quality after 8 days. However, the diode keeps the same transmittance even after 8 days.

III.3.3.2. Band Gap and Urbach Energy

From the transmittance spectra, the indirect Eg optical gaps and Urbach energy Eu for the ZnO films were deduced according to the method described in chapter II.

Following tables III.3 summarize the variation of Eg and Eu respectively in ITO substrate:

Table III-2: Variation of Eg and Eu respectively in ITO substrate.

	Eg optical gaps (eV)	Urbach energy Eu (eV)
ZnO pure	3.25	0.059
ZnO: Ga 4at. %	3.27	0.010
ZnO: Al+In 8at. %	3.01	0.095

Ga-doped ZnO and Al-In co-doped ZnO thin films deposited on ITO substrate significantly affect their optical properties. The Ga doping increases slightly the optical band gap (3,27eV) in comparison with pure ZnO gap (3,25 eV). The optical band gap is decreases remarkably for co-doped ZnO thin films (3,01 eV).

The increases of Eg gap for doped films is because the Al, In, and Ga dopants results in a higher carrier concentration. It is a well-known fact that replacing Al^{3+}, Ga^{+3}, and In^{+3} with Zn^{2+} ions results in an extra free electron [80] as seen from the equation:

$$Al_3+ \rightarrow Al_2+ + e^-$$

The increase in free carrier concentration results in the liberation of electrons that fill the low energy levels beneath the conduction band. These occupying electrons push the Fermi level towards the conduction band, thereby enlarging the forbidden energy range in ZnO thin films [81-82] The widening of the band gap is also attributed to the shrinkage of the average particle size [83].

The figure (III-10) shows the variation of the Urbach energy for pure and doped ZnO films deposited on ITO substrate. The Ga-doped ZnO presents an improved crystalline quality and reduced disorder. Conversely, Al+In doping decreases the optical band gap and increases the Urbach energy, which indicating increased disorder.

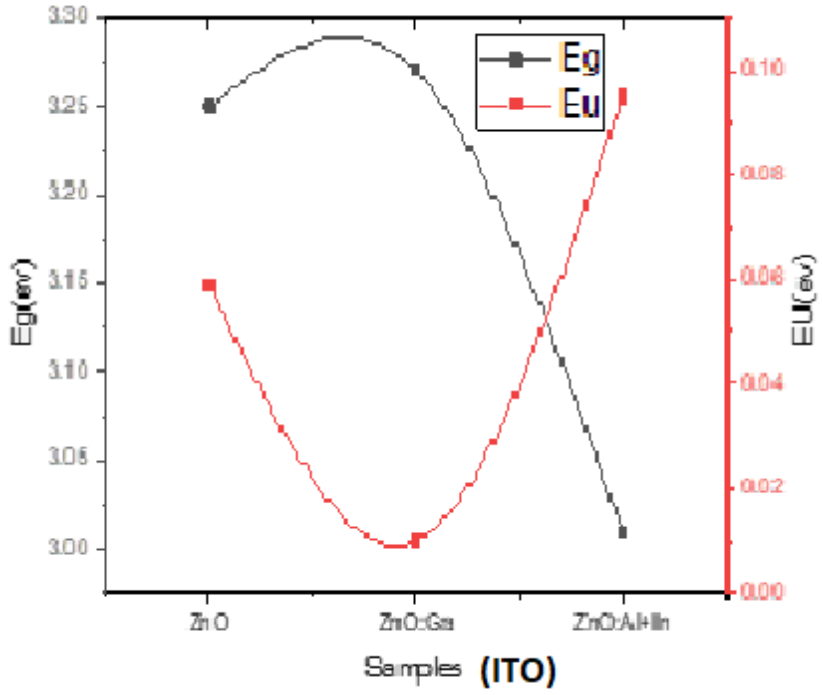

Figure III-10:variation of Eg and Eu respectively in ITO substrate.

Following tables III.4 summarize the variation of Eg and Eu of the ZnO films elaborated on Glass substrate:

Table III-3: Variation of Eg and Eu respectively in glass substrate.

	Eg optical gaps (eV)	Urbach energy Eu (eV)
ZnO pure	2.027	0.902
ZnO: Ga 4at. %	3.261	0.011
ZnO: Al+In 8at. %	3.268	0.010

Ga-doped ZnO and Al-In co-doped ZnO significantly improves its optical properties by increasing the optical band gap and reducing the Urbach energy. These enhancements indicate a higher crystalline quality and reduced disorder in the doped ZnO films, making them more

suitable for applications requiring high optical transparency and stability, such as in optoelectronic devices and transparent conductive oxides.

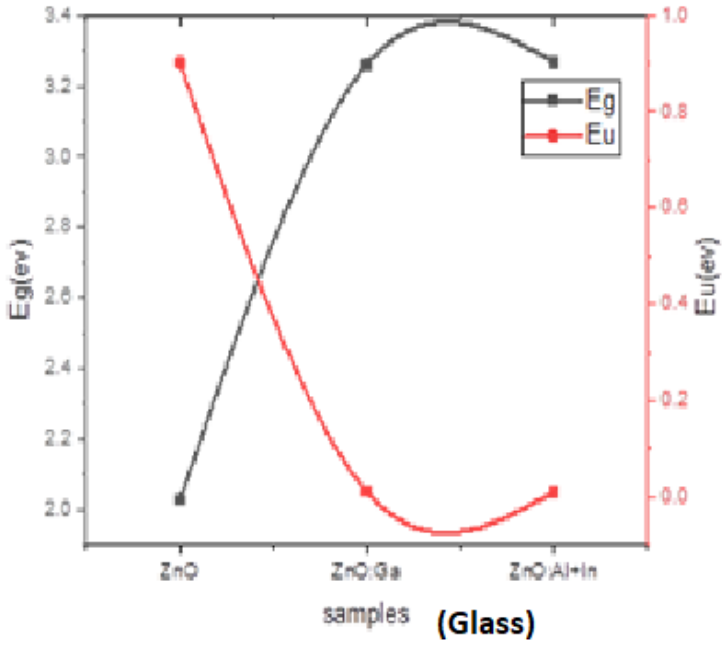

Figure III-11:variation of Eg and Eu respectively in Glass substrate.

III.3.4. Electrical Properties

III.3.4.1. The four-point characteristics

The variation in electrical conductivity and sheet resistance of ZnO films have been measured by the four-point method on a glass substrate in various samples as shown in Figure III.12 and Table III.5:

Table III-4: Values of conductivity, sheet resistance and the resistivity of ZnO thin films samples glass.

	Samples	R_{sh_moy} x10^3(Ω)	ρ x10^3 (Ω.cm)	σ x10^{-3} (Ω.cm)$^{-1}$
Verre	ZnO Pure	140,11	5,423	0,18442505
	ZnO: Ga 4at. %	2242,41	0,134	7,469
	ZnO: Al+In 8at. %	275,46	0,019	52,23408

Pure ZnO shows high resistivity and low conductivity, indicating it is less effective for applications requiring high electrical conductivity. Doping ZnO with 4% Ga significantly increases the conductivity compared to pure ZnO, although the sheet resistance is very high. This suggests that Ga doping improves the electrical properties but the film still has room for optimization. Doping ZnO with a combination of 8% Al and In leads to a significant decrease in resistivity and an increase in conductivity. This combination appears to be the most effective among the samples for enhancing electrical properties, making it potentially more suitable for applications requiring higher conductivity.

This decrease in resistance (fig. III-13) is due to the increase in carrier material concentration resulting from the addition of Al, In and Ga, which leads to the formation of more conduction electrons and oxygen vacancies.

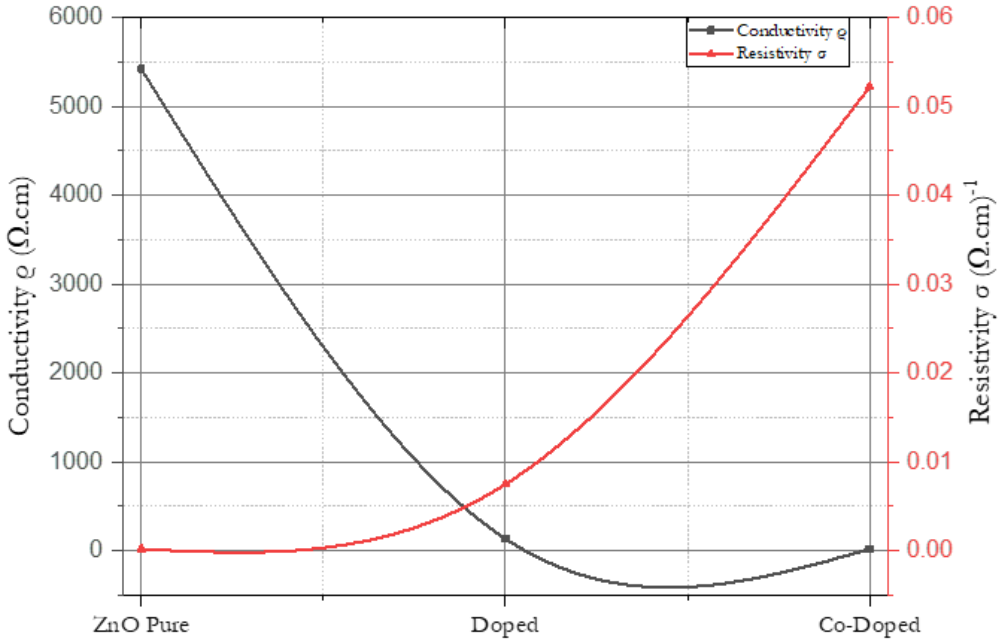

Figure III-12:The values of the sheet resistivity and the conductivity of ZnO films.

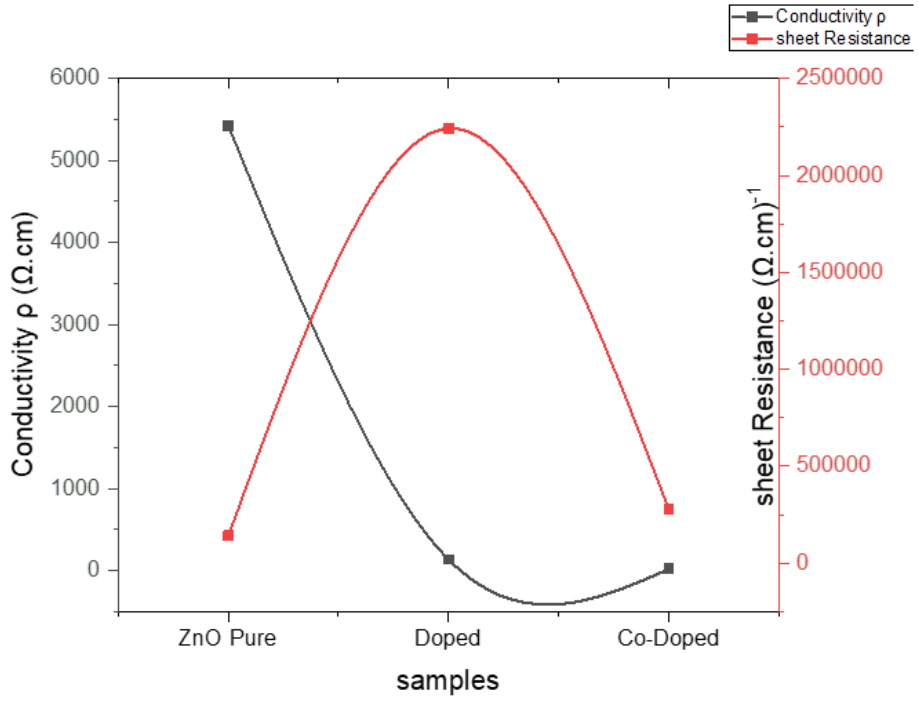

Figure III-13: The values of the sheet resistance and the conductivity of ZnO films.

Doping ZnO thin films with elements such as Ga, Al, and In substantially improves their electrical properties. Among the samples, ZnO doped with a combination of Al and In shows the most promising results in terms of increased conductivity and decreased resistivity. This suggests that careful selection and combination of dopants can tailor the electrical properties of ZnO thin films for specific applications in optoelectronics and other fields

III.3.4.2. The I–V characteristics

The I–V characteristics of the samples were measured with a B 1500 A semiconductor device analyzes system. The current–voltage data were obtained by applying voltages between 5 V and - 5V to the silver electrode (superior), whereas the inferior electrode (ITO) was grounded. The results are shown in Figures III-14 and III-15:

At low voltage in (a), the current of the diode increases exponentially with the increase in the forward voltage. In (b), the semi-logarithmic graph of the current with forward bias voltage quickly becomes dominated by the series resistance of the semiconductor, provoking the curvature of the graph for high currents. The diode shows a Schottky-type behavior, and the current originates mainly from the thermionic emission of carriers.

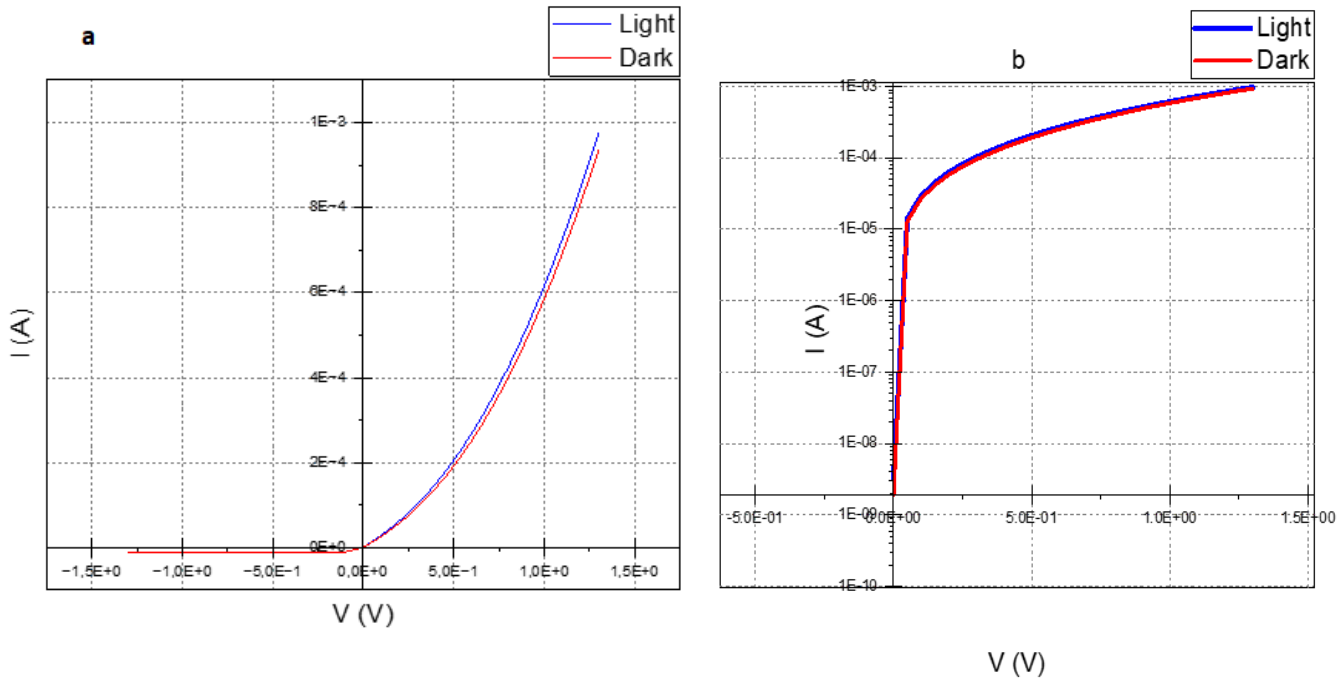

Figure III-14: Current–voltage characteristics of the diode sample in (a) forward and reverse polarization in linear scale and (b) semi-logarithmic scale (New solution: solution have been used after 24 hour).

The sight difference between the I-V diode characteristic in light and darkness is due to low luminous intensity. This means that the charge density generated under light is not significantly higher than the total amount of free electrons moving in dark conditions under the effect of the electric field applied between the semiconductors [84].

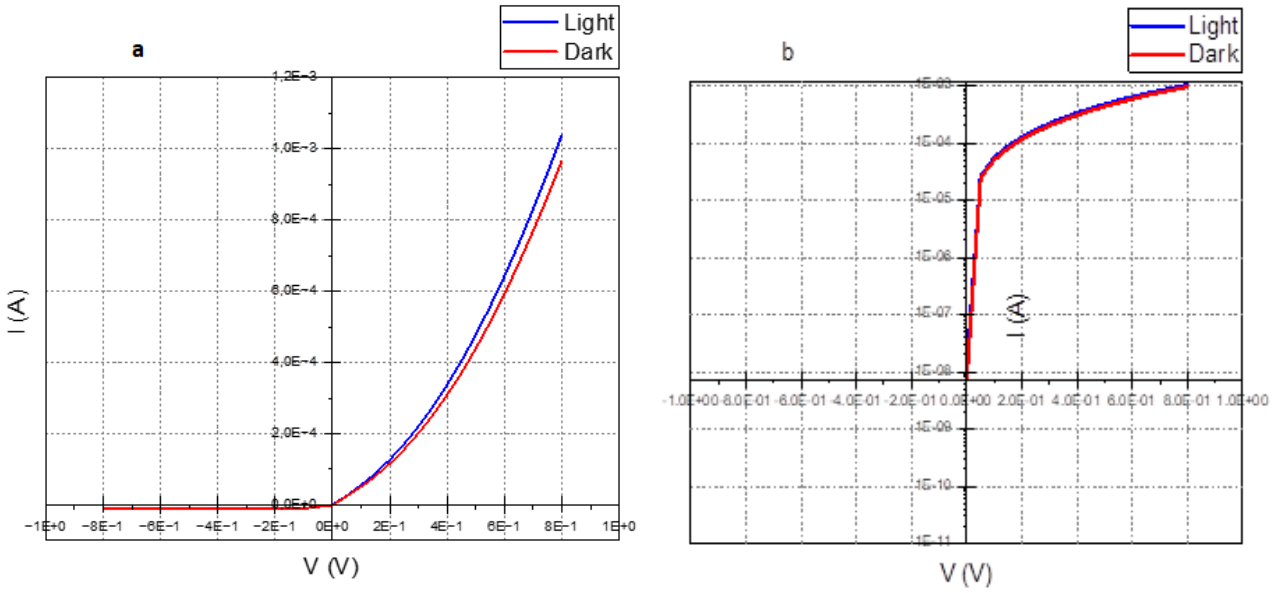

Figure III-15:Current–voltage characteristics of the diode sample in (a) linear scale and (b) semi-logarithmic scale (Old solution: solution have been used after 8 days).

Following table III.6 summarize the variation of Series resistance and Saturation current and ideality factor, Barrier height of the samples for the forward biased Ag electrode:

Table III-5:variation of Series resistance and Saturation current and ideality factor, Barrier height of the samples for the forward biased Ag electrode.

samples	R_s		η		I_s		Φ_B	
	Dark	Light	Dark	Light	Dark	Light	Dark	Light
New Solution	250	270	2.788	2.784	3.30×10^{-9}	1.94×10^{-9}	0.773	0.786
Old Solution	175.438	175.449	2.708	2.712	7.65×10^{-9}	1.21×10^{-8}	0.752	0.740

comparing two solutions, "New Solution" and "Old Solution," in terms of their characteristics under forward biased Ag electrode conditions. The table shows variations in series resistance (Rs), saturation current (Is), and ideality factor (η), as well as barrier height (ΦB) for both "Dark" and "Light" conditions.

General Conclusion

We have been fabricated a pure, doped ZnO with Ga 8% and co-doped with (Al4%, In 4%). The doped ZnO films have been used in the elaboration of ZnO-based Schottky diode via the deposition of a ZnO film co-doped with Al + In (4 at. %) on a gallium-doped ZnO film (8 at. %). The diode is deposited on ITO substrate. Each film was prepared by layering coatings by sol–gel deposition. The finished diode consists of the combination of seven layers. The total thickness of the diode is around 850 nm. The films were previously studied and structurally, optically and electrically characterized.

Additionally, and for comparative purposes, we have been fabricated and characterized un-doped ZnO films, and We have studied the effect of the substrate (ITO, Glass) and gel time (two Schottky diodes).

From the results obtained during the various characterizations carried out and the corresponding discussions, it can be concluded that:

X-ray diffraction study shows that all the films prepared in this work have polycrystalline hexagonal wurtzite phase structure.

The energy bandgap values of the un-doped films, mono-doped films, and co-doped films deposited on ITO substrate were 3.25 eV, 3.27 eV, and3.01 eV, respectively. The spectra show that all the films and the diode have a high transparency (>90%) in the visible region, and high absorption (almost 100%) in the UV region. The transmittance decreases slightly with different doping elements.

The variation in electrical conductivity and sheet resistance of ZnO the un-doped films, mono-doped films, and co-doped films were have been measured by the four-point method on a glass substrate, The electrical resistivity values obtained were (5.423 ,0.134,0.019) * 10^3 Ω.cm.

The junction diodes were built by depositing layers of the high-resistivity material (ZnO: Ga) on ITO conductor substrates, followed by the deposition of layers of the low-resistivity material (ZnO: Al + In). The I–V characteristics of these diodes were analyzed in terms of gel time. The results show a Schottky-type behavior in the dark and under light, which is controlled by the thickness of the resistive layer. From the I–V curves, the characteristic parameters including barrier height, ideality factor, and series resistance were calculated.

The results presented here indicate that an optimized thickness of the resistive layer must be obtained in order to achieve the maximum performance of the diode.

REFERENCES

[1] ADEDOKUN, O. (2018). Review on Transparent Conductive Oxides Thin Films deposited by Sol-gel spin coating technique. *International Journal of Engineering Science and Application*, *2*(3), 88-97.

[2] Özgür, Ü., Hofstetter, D., &Morkoc, H. (2010). ZnO devices and applications: a review of current status and future prospects. *Proceedings of the IEEE*, *98*(7), 1255-1268.

[3] Habis, C., Zaraket, J., &Aillerie, M. (2022, July). Transparent Conductive Oxides. Part II. Specific Focus on ITO, ZnO-AZO, SnO2-FTO Families for Photovoltaics Applications. In Defect and Diffusion Forum (Vol. 417, pp. 257-272). Trans Tech Publications Ltd.

[4] Hernández-Ochoa, M. A., Arizpe-Chávez, H., Ramírez-Bon, R., Pérez-Rodríguez, A., Cortez-Valadez, M., & Flores-Acosta, M. (2019). Current–voltage characterization of transparent ITO/ZnO/ZnO:(Al + In)/Ag Schottky diodes prepared with multilayer films by sol–gel deposition. *Journal of Electronic Materials.* Advance online publication. https://doi.org/10.1007/s11664-019-07880-6

[5] Han, K. J., Kang, K. S., Chen, Y., Yoo, K. H., & Kim, J. (2009). Effect of annealing temperature on the conduction mechanism for a sol–gel driven ZnO Schottky diode. Journal of Physics D: Applied Physics, 42(12), 125110

[6] Stadler, A. (2012). Transparent conducting oxides—An up-to-date overview. *Materials*, *5*(4), 661-683. https://doi.org/10.3390/ma5040661

[7] Rahmane, S. (2008). *Elaboration et caractérisation de couches minces par spray pyrolyse et pulvérisation magnetron* (Doctoral dissertation, U. Mohamed Kheider - Biskra).

[8] Garnier, J. (n.d.). *Elaboration de couches minces d'oxydes transparents et conducteurs par spray CVD assisté par radiation infrarouge pour applications photovoltaïques*. Retrieved from https://pastel.hal.science/pastel-00005629

[9] Allag, A. (2018). Optimisation des conditions d'élaboration des couches minces d'oxyde d'étain SnO2 par spray (Doctoral dissertation, Université Mohamed Khider–Biskra).

[10] Yadav, A. A., Masumdar, E. U., Moholkar, A. V., Neumann-Spallart, M., Rajpure, K. Y., & Bhosale, C. H. (2009). Electrical, structural and optical properties of SnO2: F

thin films: Effect of the substrate temperature. *Journal of Alloys and Compounds, 488*(1), 350-355. https://doi.org/10.1016/j.jallcom.2009.08.130

[11] Assi, A. A., & Saleh, W. R. (2014). Conductive polymer dye-sensitive solar cell (DSSC) for improving the efficiency (PhD dissertation). University of Baghdad.

[12] Launey, J., & Tosser, A. (1976). Couches conductrices et transparentes obtenues par pulvérisation d'une cible de SnO2. *Active and Passive Electronic Components, 2*, 223-231.

[13] Godinho, K. G., Carey, J. J., Morgan, B. J., Scanlon, D. O., & Watson, G. W. (2010). Understanding conductivity in SrCu2O2: Stability, geometry and electronic structure of intrinsic defects from first principles. *Journal of Materials Chemistry*, *20*(6), 1086–1096. https://doi.org/10.1039/b921061j

[14] Boulmelh, S. (2015). Élaboration et caractérisation d'un dépôt de couches minces d'oxyde de zinc par spray pyrolyse. Mémoire non publié,

[15] Mezhoud, W., & Bounib, H. E. (2020). Équilibrage d'un rotor multidisque [Doctoral dissertation, Université de Jijel].

[16] Khelifi, C. (2018). Tin dioxide (SnO2) thin films deposited by ultrasonic spray technique: Properties and applications (Doctoral dissertation). University of Med Khider Biskra.

[17] Introduction to Nanomaterials. (2011). Retrieved from https://www.researchgate.net/publication/259118068

[18] oumezoued, A. (2020). Étude et préparation par sol-gel de nanomatériaux à base d'oxydes semiconducteurs et leurs applications [Study and preparation of semiconductor oxide-based nanomaterials by Sol-Gel method and their applications]. (Doctoral dissertation)

[19] Bekhti, W. (n.d.). Synthèse par voie hydrothermale et caractérisation des micro/nanostructures d'Oxyde de Zinc [Thèse de doctorat, Université ORAN I Ahmed Ben Bella, en co-tutelle avec l'Université Claude Bernard LYON I].

.

[20] Sari, A., & Bousharit, S. (2017). Élaboration et caractérisation des couches minces d'oxyde de cuivre non dopé [Elaboration and characterization of undoped copper oxide thin films] (Doctoral dissertation).

[21] Zoubiri, B. . (2022). دراسة خصائص الشرائح الرقيقة لأكسيد الزنك المحضرة بطريقة الرش بالهواء المضغوط انطلاقا من مصادر مختلفة للزنك (مذكرة ماستر).

[22] Benkhetta, Y. (2018). Elaboration and characterization of thin layers of zinc oxide (ZnO) deposited by ultrasonic spray for photovoltaic and optoelectronic applications. Master's thesis, U. Mohamed Khider of Biskra,

[23] Mühlbacher, M. (2015). High-resolution characterization of TiN diffusion barrier layers. Linköping University Electronic Press. https://doi.org/10.3384/lic.diva-120394

[24] Bouaichi, F. (2018). Deposition and analysis of Zinc Oxide thin films elaborated using spray pyrolysis for photovoltaic applications. Mohamed Khider University of Biskra,

[25] Khaoula, S., Abdelghni, M. A., & Kanza, M. A. (n.d.). The development and characterization of pure and doped ZnO nanopowder with Ga and Bi via the sol-gel method. Master's thesis, Jury: MASTER MEMORY.

[26] Young, S.-J., Yang, C.-C., & Lai, L.-T. (2017). Review—Growth of Al-, Ga-, and In-Doped ZnO Nanostructures via a Low-Temperature Process and Their Application to Field Emission Devices and Ultraviolet Photosensors. *Journal of the Electrochemical Society*, *164*(5), B3013-B3028. https://doi.org/10.1149/2.0051705jes

[27] Yilmaz, M. (2015). Investigation of characteristics of ZnOnanocrystalline thin films with varying dopant content. *Materials Science in Semiconductor Processing*, *40*, 99–106. https://doi.org/10.1016/j.mssp.2015.06.031

[28] Maache, A. (2021). Elaboration et caractérisation optique des couches minces de ZnO dopé ou Co-dopé obtenues par méthode sol-gel (Doctoral dissertation). Université Ferhat Abbas Sétif 1.

[29] Herissi, L. (2008). Élaboration par pulvérisation pyrolytique et caractérisation de couches minces semi-conductrices et transparentes d'oxyde de zinc: Perfectionnement du système de dépôt [Pyrolytic spray deposition and characterization of semiconductor

and transparent thin films of zinc oxide: Improvement of the deposition system]. Magister thesis, Université Larbi ben M'hidi-Oum el Bouaghi, Algeria..

[30] Talbi, F., & Ferhat, L. (Date non spécifiée). Conception et réalisation d'un spin coater pour le dépôt en couches minces (Mémoire de fin d'étude de master académique, Spécialité: Electronique, Filière: Electronique Biomédicale). Université Mouloud Mammeri

[31]] N. Abdelouahab, Preparation and characterization of thin films nanostructures based on ZnO and other oxides. Doctoral Thesis, University of Oum El Bouaghi, Algeria (2019).

[32] Mohamed, D. (2019). Preparation and characterization of titanium dioxide and zinc oxide thin films for optoelectronic applications using the sol-gel (spin coating) technique.

[33] Nassiba, A., Chemsa, A., Mí°šˆd, S., & Pr, R. (n.d.). Elaboration and Characterization of Copper Oxide Thin Films on Zinc Oxide Substrates (CuO / ZnO) by Chemical Bath.

[34] Lakhdar, B., Abdallah, A., Nadjette, H., & Kheira, B. (n.d.). The effect of bromine doping rate on the properties of ZnO thin films. Master's thesis

[35] Hamani, N. (2021). Elaboration et caractérisation des couches minces d'oxyde d'indium dopées à l'étain et au brome obtenue par spray pyrolyse ultrasonique (Doctoral dissertation, Université de mohamed kheider biskra).

[36] Mohamed, O. (2017). Synthesis and characterization of zinc oxide (ZnO) thin films deposited by spray pyrolysis for applications in electronics and photonics. Master's thesis, Mohamed Khider University of Biskra

[37] Vyas, S. (2020). A short review on properties and applications of zinc oxide based thin films and devices: ZnO as a promising material for applications in electronics, optoelectronics, biomedical and sensors. *Johnson Matthey Technology Review, 64*(2), 202-218. https://doi.org/10.1595/205651320X15694993568524

[38] Dey, A. (2018). Semiconductor metal oxide gas sensors: A review. *Materials Science and Engineering: B, 229*, 206–217. https://doi.org/10.1016/j.mseb.2017.12.036

[39] Chang, M. H., Das, D., Varde, P. V., & Pecht, M. (2012). Light emitting diodes reliability review. *Microelectronics Reliability, 52*, 762–782. https://doi.org/10.1016/j.microrel.2011.07.063

[40] Choi, J., Woo, H. J., Kim, S., Sun, J., Kang, M. S., Song, Y. J., Cho, J. H. (2020). Schottky junction photodiode based on graphene—organic semiconductor heterostructure. *Journal of Industrial and Engineering Chemistry, 89*, 233–238. https://doi.org/10.1016/j.jiec.2020.05.018.

[41] ang, Y., Sun, X. W., Tay, B. K., You, G. F., Tan, S. T., Teo, K. L. (2008). A p-n homojunction ZnO nanorod light-emitting diode formed by As ion implantation. *Applied Physics Letters, 93*. https://doi.org/10.1063/1.3054639

[42] Bacela, J., Łabowska, M. B., Detyna, J., Ziety, A., & Michalak, I. (2020). Functional coatings for orthodontic archwires-A review. *Materials, 13*. https://doi.org/10.3390/MA13153257.

[43] Saida, M. M., Attaf, M., Pr, A., Saidi, M., Pr, H., & OUISSAL LATRA, H. (n.d.). Effect of PH precursor on properties of TiO2 thin films deposited by ultrasonic spray process and their photocatalytic applications. In *Master Memory Jury* (Chair),

[44] Shahidi, S., Moazzenchi, B., & Ghoranneviss, M. (2015). A review-application of physical vapor deposition (PVD) and related methods in the textile industry. *EPJ Applied Physics, 71*.https://doi.org/10.1051/epjap/2015140439.

[45] Patel, A. J. (2022). Synthesis and characterization of pure and doped ZnO thin films by colloidal solution route.

[46] Kökbudak Baldan, G. (2023). Optimization of novel passivation and carrier selective layers on crystalline silicon solar cell technologies.

[47] Spear, K. E. (1982). Principles and applications of chemical vapor deposition (CVD).

[48] Zhao, D. (2023). Transparent conducting oxides and other functional thin films grown via aerosol assisted chemical vapour deposition (Doctoral dissertation, UCL (University College London)).

[49] Mann, S., Burkett, S. L., Davis, S. A., Fowler, C. E., Mendelson, N. H., Sims, S. D., ... &Whilton, N. T. (1997). Sol− gel synthesis of organized matter. Chemistry of materials, 9(11), 2300-2310

[50] Danks, A. E., Hall, S. R., & Schnepp, Z. J. M. H. (2016). The evolution of ‘sol–gel’chemistry as a technique for materials synthesis. Materials Horizons, 3(2), 91-112.

[51] Bahadur, H., Srivastava, A. K., Sharma, R. K., & Chandra, S. (2007). Morphologies of sol-gel derived thin films of ZnO using different precursor materials and their

nanostructures. *Nanoscale Research Letters, 2,* 469–475. https://doi.org/10.1007/s11671-007-9089-x.

[52] Sottmann, J., Pralong, V., Barrier, N., & Martin, C. (2019). An electrochemical cell for operando bench-top X-ray diffraction. Journal of Applied Crystallography, 52(2), 485-490.

[53] Adl, A. H. (n.d.). Synthesis and Characterization of Solution Processed ZnO Thin Films. Unpublished doctoral dissertation, University of Alberta, Department of Electrical and Computer Engineering.

[54] Maache, M. (2014). Elaborattion de films Minces d'oxydes Semiconducteurs Par Voie sol-Gel (Doctoral dissertation, Université Mohamed Khider Biskra).

[55] Yang, L. (2005). Fabrication and characterization of microlasers by the sol-gel method (Doctoral dissertation).

[56] Brella, M. (2022). Elaboration et Caractérisations de Semi-conducteurs Transparents en Couches Minces Pour Applications Technologiques [Doctoral dissertation, Université Kasdi Merbah Ouargla].

[57] Rabaste, S. (2003). Microcavités optiques élaborées par voie sol-gel: applications aux ions terre rare d'Eu^3+ et aux nanocristaux semiconducteurs de CdSe [Optical microcavities elaborated by sol-gel method: applications to rare earth ions of Eu^3+ and semiconductor nanocrystals of CdSe] (Doctoral dissertation, Université Claude Bernard-Lyon I).

[58] Othmane, M. (2017). Synthesis and characterization of zinc oxide (ZnO) thin films deposited by spray pyrolysis for applications in electronics and photonics. Université de Biskra

[59] N. Kouidri, S. Rahmane, A. Allag, (2019) Substrate temperature-dependent properties of sprayed cobalt oxide thin films, Journal of Materials Science: Materials in Electronics 30 1153–1160. https://doi.org/10.1007/s10854-018-0384-3.

[60] Hafdallah, A., Derrar, K., Aida, M. S., & Attaf, N. (2016). Effet de la solution précurseur sur les propriétés structurales et optiques des couches minces de ZnO préparées par spray pyrolyse. *Afrique Science, 12*(3).

[61] Kouidri, N. (2019). Contribution à l'étude de couches minces d'oxydes transparents conducteurs à base de zinc et cobalt par spray pneumatique [Contribution to the study

of transparent conducting oxide thin films based on zinc and cobalt by pneumatic spray] (Doctoral dissertation). University of Mohamed Khider, Biskra.

[62] Maache, A. (2021). Elaboration et caractérisation optique des couches minces de ZnO dopé ou Co-dopé obtenues par méthode sol-gel (Doctoral dissertation, Université Ferhat Abbas Sétif 1, Faculté des Sciences, Département de Physique).

[63] Tabet, A. (2013). Optimisation des conditions d'élaboration (température de substrat et distance bec-substrat) des films minces de ZnO par spray (Doctoral dissertation, Université Mohamed Khider-Biskra).

[64] Benrabah, B. (2010). Etude des Propriétés Physico-chimiques des Couches de SnO2 Préparées par la Technique «dip-coating (Doctoral dissertation, Universite mohamed boudiaf'des sciences et de la technologie d'oran).

[65] Yousra, K., Temam, E. G., Saâd, R., & Barkat, H. (2023). Effect of film thickness on the electrical and the photocatalytic properties of ZnO nanorods grown by SILAR technique. Physica Scripta, 98(12), 125954.

[66]] Attaf, A., Djadai, A., Derbali, A., Saidi, H., Aida, M. S., Lehraki, N., ... & Poulain, M. (2022). The effect of ultrasonic wave amplitude on the physical properties of zinc oxide (ZnO) deposited by ultrasonic spray method. Materials Science and Engineering: B, 275, 115525

[67] Attaf, A., Derbali, A., Saidi, H., Bouhdjer, A., Aida, M. S., Messemeche, R., ... &Djehiche, N. E. (2022). Precursor concentration effect on the physical properties of transparent titania (Anatase-TiO2) thin films grown by ultrasonic spray process for optoelectronics application. Optical Materials, 132, 112790

[68] CHEICK SID, E. S. (2019). Etude et simulation AC des caractéristiques électriques de quelques cellules solaires en couches minces (Doctoral dissertation, Université Ibn Khaldoun-Tiaret-).

[69] Benhamida, S. (2018). Caractérisation Des Couches Minces D'oxyde De Nickel (NiO) Elaboré Par Spray Pyrolyse (Doctoral dissertation, Université Mohamed Khider-BISKRA).

(70] Ziani, N. (2020). Etude et élaboration d'hétérojonction Si-OTC pour la réalisation de dispositifs photovoltaïques (Doctoral dissertation, UNIVERSITE MOULOUD MAMMERI TIZI-OUZOU).

[71]Keithley Instruments. (2013). Easy I-V characterization of diodes using the Model 2450 SourceMeterSMU instrument (Number 3225). Retrieved from http://www.keithley.com/company/buy

[72] Boulgamh, F., Telia, A., Remram, M., & Djouambi, A. (2005). IV and CV methods to extract Al/polysilicon Schottky diode parameters. In *Proceedings of the 7th WSEAS International Conference on Mathematical Methods and Computational Techniques In Electrical Engineering* (pp. 245-248).

[73] Jana, S., Mandal, S., Roy, S., Saifuddin, M., & Hazra, S. (2024). Sputter-cleaning modified interfacial energetic and molecular structure of DNTT thin film on ITO substrate. Applied Surface Science, 652, 159368.

[74]Askari, H., Fallah, H., Askari, M., &Mohmmadieyh, M. C. (2014). Electrical and optical properties of ITO thin films prepared by DC magnetron sputtering for low-emitting coatings. arXiv preprint arXiv:1409.5293.

[75] Zhang, Y., Li, Q., Tian, Z., Hu, P., Qin, X., & Yun, F. (2020). Gas-sensing properties of ITO materials with different morphologies prepared by sputtering. SN Applied Sciences, 2, 1-11.

[76]Guillén, C., & Herrero, J. (2008). Structural, optical and electrical characteristics of ITO thin films deposited by sputtering on different polyester substrates. Materials Chemistry and Physics, 112(2), 641-644.

[77] Karthika, K., & Ravichandran, K. (2015). Tuning the microstructural and magnetic properties of ZnO nanopowders through the simultaneous doping of Mn and Ni for biomedical applications. Journal of Materials Science & Technology, 31, 1111–1117. https://doi.org/10.1016/j.jmst.2015.09.001.

[78] Amri, A., Arab, L., Meftah, A., & Latif, A. (2023). Effect of aluminum doping on the structural, optical, and electrical properties of ZnO thin films processed under thermal shock conditions. *Journal of Results in Optics, 11*, 100426. https://doi.org/10.1016/j.rio.2023.100426

[79] Wells, A.F. (1984). Structural Inorganic Chemistry (5th ed.). Oxford: Clarendon Press. (metallic radii for 12-coordination); Huheey, E. A. (1976). Inorganic Chemistry:

Principles of Structure and Reactivity (1st ed.). New York: Harper & Row. (covalent radii for nonmetals); Shannon, R.D. (1976). Acta Crystallographic Section A: Foundations of Crystallography, 32, 751. (ionic radii for 6-coordination)

[80] Akdağ, A., Budak, H. F., Yılmaz, M., Efe, A., Büyükaydın, M., Can, M., Turgut, G., & Sönmez, E. (2016). Structural and morphological properties of Al-doped ZnO nanoparticles. *Journal of Physics: Conference Series, 707*. https://doi.org/10.1088/1742-6596/707/1/012020

[81] Garcés, F. A., Budini, N., Arce, R. D., & Schmidt, J. A. (2015). Effect of thickness on structural and electrical properties of Al-doped ZnO films. *Thin Solid Films, 574*, 162–168. https://doi.org/10.1016/j.tsf.2014.12.013.

[82] Srinatha, N., Raghu, P., Mahesh, H. M., & Angadi, B. (2017). Spin-coated Al-doped ZnO thin films for optical applications: Structural, micro-structural, optical, and luminescence studies. *Journal of Alloys and Compounds, 722*, 888–895. https://doi.org/10.1016/j.jallcom.2017.06.182.

[83] He, H.-Y., Huang, J.-F., Fei, J., & Lu, J. (2015). La-doping content effect on the optical and electrical properties of La-doped ZnO thin films. *Journal of Materials Science: Materials in Electronics, 26*(3), 1205–1211. https://doi.org/10.1007/s10854-014-2526-6.

ANNEXES

ASTM Sheets For The ZnO wurtzite Phase

Name and formula

Reference code:	01-075-0576
Compound name:	Zinc Oxide
ICSD name:	Zinc Oxide
Empirical formula:	OZn
Chemical formula:	ZnO

Crystallographic parameters

Crystal system:	Hexagonal
Space group:	P63mc
Space group number:	186
a (Å):	3.2427
b (Å):	3.2427
c (Å):	5.1948
Alpha (°):	90.0000
Beta (°):	90.0000
Gamma (°):	120.0000
Calculated density (g/cm^3):	5.71
Volume of cell (10^6 pm^3):	47.31
Z:	2.00
RIR:	5.53

Subfiles and quality

Subfiles:	Alloy, metal or intermetalic Corrosion ICSD Pattern Inorganic Pharmaceutical
Quality:	Calculated (C)

Comments

ICSD collection code:	029272
Creation Date:	1/1/1970
Modification Date:	1/1/1970
ICSD Collection Code:	029272
Temperature Factor:	ITF. The Wurtzite Z Parameter for Beryllium Oxide and Zinc Oxide. b2 (P63MC). AX.

References

Primary reference: *Calculated from ICSD using POWD-12++*, (1997)
Structure: Sabine, T.M., Hogg, S., *Acta Crystallography., Sec. B*, **25**, 2254, (1969)

Peak list

No.	h	k	l	d [A]	2Theta[deg]	I [%]
1	1	0	0	2.80826	31.840	56.2
2	0	0	2	2.59740	34.503	41.2
3	1	0	1	2.47039	36.337	100.0
4	1	0	2	1.90683	47.653	21.5
5	1	1	0	1.62135	56.731	30.9
6	1	0	3	1.47393	63.016	27.2
7	2	0	0	1.40413	66.541	4.1
8	1	1	2	1.37538	68.120	22.7
9	2	0	1	1.35549	69.261	11.2
10	0	0	4	1.29870	72.759	1.8
11	2	0	2	1.23520	77.162	3.5
12	1	0	4	1.17875	81.610	1.8
13	2	0	3	1.09063	89.868	7.1

Stick Pattern

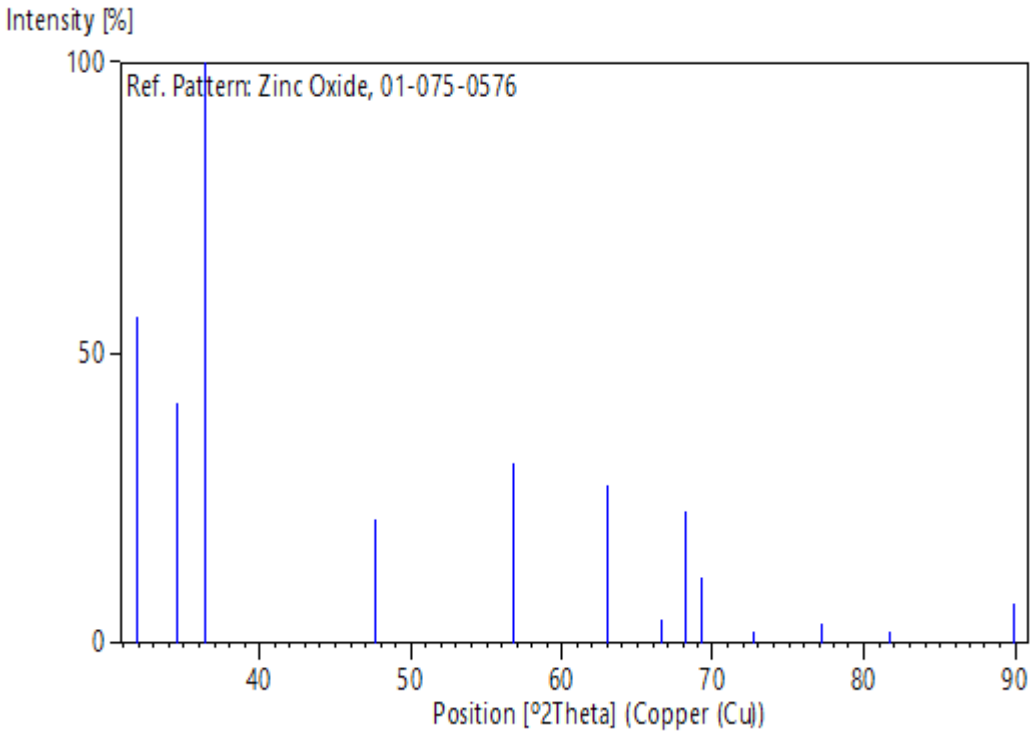

ASTM Sheets For The ITO

Name and formula

Reference code:	01-089-4598
Compound name:	Indium Tin Oxide
ICSD name:	Indium Tin Oxide
Empirical formula:	$In_{1.88}O_3Sn_{0.12}$
Chemical formula:	$(In_{1.88}Sn_{0.12})\ O_3$

Crystallographic parameters

Crystal system:	Cubic
Space group:	Ia-3
Space group number:	206
a (Å):	10.1309
b (Å):	10.1309
c (Å):	10.1309
Alpha (°):	90.0000
Beta (°):	90.0000
Gamma (°):	90.0000
Calculated density (g/cm^3):	7.11
Volume of cell (10^6 pm^3):	1039.79
Z:	16.00
RIR:	13.02

Subfiles and quality

Subfiles:	Corrosion ICSD Pattern Inorganic
Quality:	Calculated (C)

Comments

ICSD collection code:	050849
Creation Date:	1/1/1970
Modification Date:	1/1/1970
ICSD Collection Code:	050849. Rietveld profile refinement applied
Temperature Factor:	ITF. Structural studies of tin-doped indium oxide (ITO) and In4 Sn3 O12. e d c b (IA3-). A2X3.

References

Primary reference:	*Calculated from ICSD using POWD-12++*
Structure:	Nadaud, N., Lequeux, N., Nanot, M., Jove, J., Roisnel, T., *J. Solid*

State Chem., **135**, 140, (1998)

Peak list

No.	h	k	l	d [A]	2Theta[deg]	I [%]
1	2	0	0	5.06545	17.494	0.3
2	2	1	1	4.13592	21.468	12.3
3	2	2	0	3.58181	24.838	0.1
4	2	2	2	2.92454	30.543	100.0
5	1	2	3	2.70760	33.057	1.3
6	4	0	0	2.53273	35.413	29.6
7	4	1	1	2.38788	37.639	5.1
8	4	2	0	2.26534	39.758	1.1
9	3	3	2	2.15992	41.787	4.3
10	4	2	2	2.06796	43.739	0.9
11	1	3	4	1.98683	45.623	7.9
12	1	2	5	1.84964	49.223	2.3
13	4	4	0	1.79091	50.950	33.1
14	4	3	3	1.73744	52.636	2.0
15	6	0	0	1.68848	54.286	0.4
16	6	1	1	1.64345	55.901	4.4
17	0	2	6	1.60184	57.486	1.0
18	5	4	1	1.56323	59.045	3.5
19	6	2	2	1.52729	60.577	23.0
20	1	3	6	1.49372	62.087	4.7
21	4	4	4	1.46227	63.577	4.3
22	5	4	3	1.43273	65.047	1.7
23	0	4	6	1.40490	66.500	1.1
24	6	3	3	1.37864	67.937	2.4
25	6	4	2	1.35380	69.360	1.3
26	1	5	6	1.28663	73.553	1.8
27	8	0	0	1.26636	74.930	2.9
28	8	1	1	1.24703	76.298	2.7
29	8	2	0	1.22855	77.658	1.6
30	6	5	3	1.21087	79.011	1.6
31	8	2	2	1.19394	80.358	1.0
32	8	3	1	1.17769	81.699	2.4
33	6	6	2	1.16209	83.036	5.1
34	2	5	7	1.14710	84.369	0.1
35	0	4	8	1.13267	85.699	3.7
36	8	3	3	1.11877	87.027	0.7
37	2	4	8	1.10537	88.353	0.8
38	6	5	5	1.09244	89.678	1.7

Stick Pattern

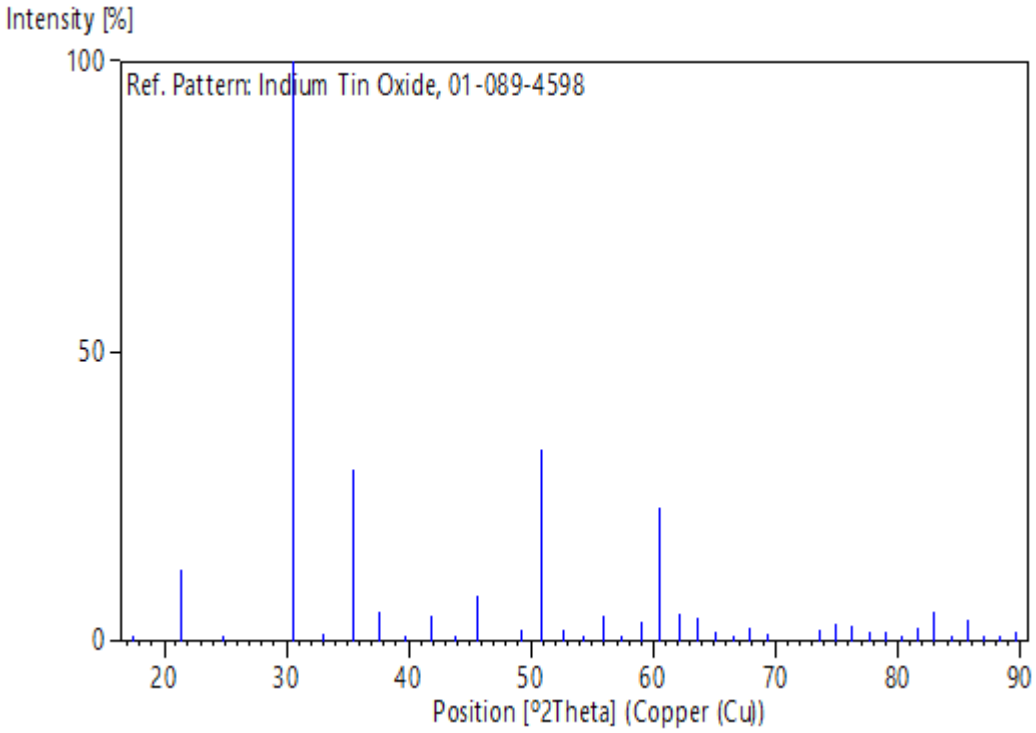
Intensity [%]
100
50
0
Ref. Pattern: Indium Tin Oxide, 01-089-4598
20
30
40
50
60
70
80
90
Position [°2Theta] (Copper (Cu))

Abstract

Preparation and Characterization of ZnO-based Schottky diode Prepared with Sol–Gel Method.

A ZnO-based Schottky diode have been fabricate via the deposition of a ZnO film co-doped with Al + In on a Gallium-doped ZnO film with sol–gel method. The XRD of the films shows a polycrystalline structure and grains size in nanoscale. The films present a high transmittance in the visible, and the I–V characteristics show a Schottky-type behavior in the dark and under light, which is controlled by the thickness of the resistive layer. and the optical properties will be analyzed with the UV-Vis spectrophotometer.

Key words: Thin films, sol–gel, ZnO, junction diodes, metal–insulator–Semicond

ملخص

تحضير وتوصيف صمام ثنائي شوتكي قائم على الزنك-أكسيد الزنك (ZnO) تم تحضيره بطريقة الهلام -المحلول.

صُنع صمام ثنائي شوتكي قائم على الزنك (ZnO) من خلال ترسيب فيلم ZnO مطعّم (Al +In) على فيلم ZnO المطعّم بالجاليوم بطريقة الهلام -المحلول. يُظهر XRD للأفلام بنية متعددة الكريستالات وحجم حبيبات بمقياس النانو. تُظهر الأفلام نفاذية عالية في الضوء المرئي، وتظهر خصائص I-V سلوكًا من نوع شوتكي في الظلام وتحت الضوء، والذي يتم التحكم فيه من خلال سمك الطبقة المقاومة.

الكلمات المفتاحية: أفلام رقيقة، الهلام-المحلول، أكسيد الزنك (ZnO) ,ثنائيات الوصلة، عازل معدني-أشباه الموصلات.

Résumé

Préparation et caractérisation d'une diode Schottky à base de ZnO préparée par la méthode Sol-Gel.

Une diode Schottky à base de ZnO a été fabriquée par le dépôt d'un film de ZnO Co-dopé avec Al + In sur un film de ZnO dopé au Gallium avec la méthode sol-gel. La XRD des films montre une structure polycristalline et des grains de taille nanométrique. Les films présentent une transmittance élevée dans le visible, et les caractéristiques I-V montrent un comportement de type Schottky dans l'obscurité et sous la lumière, qui est contrôlé par l'épaisseur de la couche résistive. Les propriétés optiques seront analysées à l'aide du spectrophotomètre UV-Vis.

Mots clés : Couches minces, sol-gel, ZnO, diodes à jonction, métal-isolant-semiconducteur

REPUBLIQUE ALGERIENNE DEMOCRATIQUE ET POPULAIRE
MINISTERE DE L'ENSEIGNEMENT SUPERIEUR
ET DE LA RECHERCHE SCIENTIFIQUE
UNIVERSITE MOHAMED KHIDER - BISKRA
Faculté des SE&SNV

الجمهورية الجزائرية الديمقراطية الشعبية
وزارة التعليم العالي والبحث العلمي
جامعة محمد خيضر بسكرة
كلية العلوم الدقيقة وعلوم الطبيعة والحياة

Département des Sciences de la matière

قسم :علوم المادة

Filière: Physique

شعبة :الفيزياء

تصريـح شرفـــي

خاص بالالتزام بقواعد النزاهة العلمية لإنجاز بحث

(ملحق القرار 1082 المؤرخ في 2021/12/27)

أنا الممضي أسفله،

السيد(ة):.....تنني تنيحياء.....

الصفة: طالب سنة ثانية ماسترفيزياء تخصص:.فيزياء المادة المكثفة

الحامل(ة) لبطاقة التعريف الوطنية رقم: 208035930 الصادرة بتاريخ:.2022-7-4

المسجل بكلية: العلوم الدقيقة وعلوم الطبيعة والحياة قسم: علوم المادة

والمكلف بانجاز أعمال بحث : مذكرة ماستر في الفيزياء

عنوانها: Preparation and characterization of ZnO based Schottky diode prepared with Sol-Gel Method

أصرح بشرفي أني ألتزم بمراعاة المعايير العلمية والمنهجية ومعايير الأخلاقيات المهنية والنزاهة الأكاديمية المطلوبة في انجاز البحث المذكور أعلاه وفق ما ينص عليه القرار رقم 1082 المؤرخ في 2021/12/27المحدد للقواعد المتعلقة بالوقاية من السرقة العلمية ومكافحتها.

التاريخ: 2024-2-22

إمضاء المعني بالأمر